AIAA JOURNAL
Vol. 45, No. 8, August 2007

Comparisons Between Experiment and Large-Eddy Simulation for Jet Noise

K. Viswanathan*
The Boeing Company, Seattle, Washington 98124-2207
M. L. Shur†
New Technologies and Services, 197198, St. Petersburg, Russia
P. R. Spalart‡
The Boeing Company, Seattle, Washington 98124-2207
and
M. Kh. Strelets§
New Technologies and Services, 197198, St. Petersburg, Russia

DOI: 10.2514/1.25892

Numerical simulations of the flowfield and the noise generated by round nozzles are carried out and analyzed, with the twin goals of gaining insight into the flow features that are responsible for noise generation and of validating large-eddy simulation in as much depth as possible. The importance of including the nozzle internal flow, especially for complex geometries of interest, is emphasized. A two-step Reynolds-averaged Navier–Stokes/large-eddy simulation methodology is developed and applied to several nozzle geometries. Results from both Reynolds-averaged Navier–Stokes and large-eddy simulation computations are presented. The spectral predictions from large-eddy simulation are in good agreement with measured data, for a wide range of jet conditions. The upper limit on the Strouhal number for accurate spectral predictions is rising from about 2 to near 5 on the best grids. Further, the change in spectral shape with increasing angle in the aft quadrant, from a broad spectral peak to a narrower one, is captured by the simulations; in contrast, classical jet noise theories have failed in this regard. The locations and the nature of the noise sources are also obtained. Valuable insight is gained from the simulation of an unheated jet with a Mach number as low as 0.4. Contrary to some prevailing conceptions, there is beaming of directional radiation to aft angles, confined to inlet angles $\geq \sim 150$ deg, and the spectra within this radiation sector have the narrower peak, just as at higher Mach numbers. The results are most encouraging, and this study is a part of ongoing efforts to better understand the flow physics and possibly derive fresh ideas including for noise control from a broad visibility of the turbulence.

I. Introduction

JET noise continues to be the dominant component of community noise during the takeoff segment, even for modern commercial aircraft. Despite significant research carried out over the last 50 years, there is no accepted complete theory for the generation and radiation of jet noise. A detailed knowledge of the entire turbulent flowfield is necessary to predict noise; there are significant challenges in accomplishing even this first step. Given that the time-dependent nature of the turbulence cannot be completely described, especially for jet flows at the high Reynolds numbers of interest, perhaps it is not surprising that there is no methodology capable of predicting the spectra at all angles and over the wide frequency range of interest to the aerospace industry. There is no consensus on the sources of jet noise either. Numerous theories have been proposed since the pioneering work of Lighthill [1]; the descriptions of the sources of jet noise have also tended to be different, depending on the formulation and the rearrangement of the Navier–Stokes equations. Therefore, there is a heavy reliance on experimental measurements, which tend to be very expensive and limited in the quantities that are measured. Nonintrusive optical techniques that permit the measurement of the turbulent fluctuations have been developed recently; however, their accuracy is limited. Even if all of the requisite flow information were known, there would still remain the twin challenges of identifying the noise sources and actually predicting the far-field noise to the required accuracy. The problem of relating subtle changes in the flowfield, say due to modifications to the nozzle geometry, to the radiated noise is formidable. As a result, the goal of achieving worthwhile and measurable noise reduction (say, more than 1 dB) through the manipulation of the turbulent flowfield (as opposed to increasing the engine bypass ratio) has proved to be elusive in spite of considerable effort in the last two decades.

Numerous recent studies have addressed the issue of turbulence-generated noise with the goals of obtaining better insights into the flow and improving our ability to predict noise. With the advances in computing capability, the use of large-eddy simulation (LES) for this purpose is becoming highly attractive. Many researchers in the United States and Europe have adopted this approach; a partial list of these may be found in [2–11]. A great variety of numerical formulations is implemented in these and other studies: different numerical algorithms and discretization schemes, a choice of boundary conditions, inflow conditions with and without artificial forcing, inclusion or omission of subgrid scale models, direct calculation of the sound field in the near field, or the use of integral methods for predicting noise in the far field, etc. There are pros and cons associated with all of these choices, and the accuracy of the final spectral predictions ultimately serves as the yardstick in the assessment of the goodness of the overall computational system. The other approach of using the steady-state solution from a Reynolds-averaged Navier–Stokes (RANS) simulation as input to a noise

Presented as Paper 2445 at the 12th AIAA/CEAS Aeroacoustics Conference, Cambridge, Massachusetts, 8–10 May 2006; received 14 June 2006; revision received 5 March 2007; accepted for publication 18 April 2007.

*Associate Technical Fellow, Aeroacoustics and Fluid Mechanics; k.viswanathan@boeing.com. Associate Fellow AIAA.
†Leading Research Scientist; mshur@rscac.spb.ru. Senior Member AIAA.
‡Senior Technical Fellow, Aeroacoustics and Fluid Mechanics; philippe.r.spalart@boeing.com.
§Principal Scientist; strelets@mail.rcom.ru.

prediction methodology suffers from severe limitations, and no practical method has emerged with accuracy high enough to constitute a tool. In most of the past LES studies (except for a rare few), the nozzle is not included. Instead, a simple inflow profile is specified. This practice is not satisfactory, especially for the geometries considered here.

For the past approximately 5 years, a project on developing computational tools for aeroacoustics applications has been underway at Boeing, in collaboration with New Technologies and Services (NTS) in St. Petersburg, Russia. One of the main goals of this project is the development of computer codes that have near general-geometry capability, so as to permit analysis of the flow and noise of realistic geometries encountered in aircraft applications. A second major objective is to have no empiricism or tunable constants and to achieve noise predictions with an accuracy of 2–3 dB over a wide frequency range with this stringent requirement. The LES methodology, coupled with the Ffowcs-Williams/Hawkings [12] (FWH) formulation, is the approach adopted. The major components of this effort and the main results have been published in three recent papers by Shur et al. [13–15]. Comprehensive descriptions of the general computational philosophy and the choices for the various constituents of the overall computational system may be found in [13–15]. An extensive list of references is also included in these papers.

Recently, Viswanathan [16,17] proposed the beveled nozzle for jet noise reduction and presented experimental evidence of significant benefit, relative to a conventional round nozzle, in the peak radiation sector. Detailed analyses of the aeroacoustic measurements from single jets in [16] indicated that the noise reduction is due to the modification of the noise generated by the large-scale turbulence structures. Recall that there is no explicit accounting for these structures in a RANS simulation. There is vectoring of the jet plume due to the beveled trailing edge, and the static pressure in the exit plane is nonuniform. Therefore, the nozzle geometry and the flow inside the nozzle must be included in the computations. Results for the beveled and dual-stream nozzles will be presented elsewhere.

In this study, the computational methods are used to elucidate the underlying physical mechanisms responsible for noise generation and radiation. One of the features of the radiated spectra, that of change in spectral shape from a broad peak at the lower polar angles (measured from the jet inlet axis) to a sharp peak at angles close to the jet axis, has received much attention in the past three decades. However, there is no explanation for this phenomenon. First, experimental data are presented, along with new analyses. The numerical simulations complement the experimental observations, by providing detailed flow information. The highest resolved Strouhal number in most simulations reported in the literature, even for other groups with larger computers allowing more than 15×10^6 grid points, is approximately 2. It should be clear that absolute predictions at full-scale engine frequencies (up to 10 KHz) are beyond the computer resources of today and will remain so for the foreseeable future. However, the simulations can provide a means to supplement experimental measurements, especially for quantities that are hard or impossible to measure. This is the intended application here, as LES provides detailed information on the flow and noise fields. This paper is organized as follows: a few experimental noise trends of current interest and their implications are presented; the scope of the simulations and a brief overview of the methodology are provided; and then the in-depth comparisons are presented.

II. Review of Some Measured Characteristics of Jet Noise

Some salient characteristics of jet noise, from a comprehensive experimental database of Viswanathan [18–20], are reviewed. As already noted, it is well known that the spectral shape changes with the radiation angle; see Fig. 18 in [16], for example. For the sake of completeness, a sample figure for a Mach number (M) jet of 1.0 at a total temperature ratio (T_t/T_a) of 3.2 is included here (see Fig. 1).

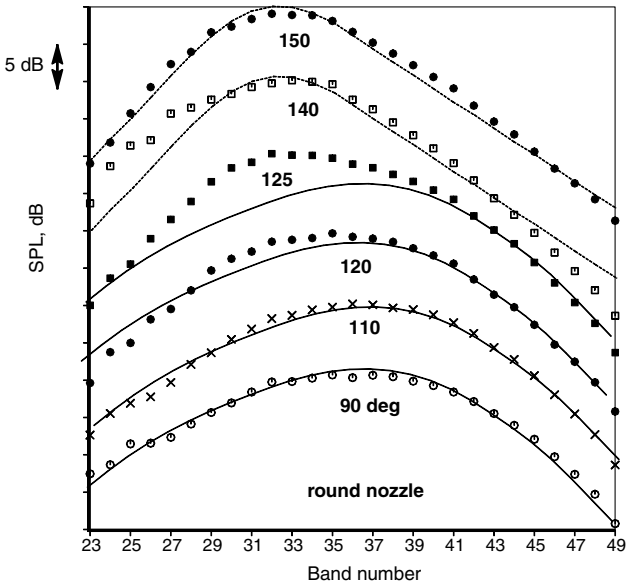

Fig. 1 Spectral shapes at different inlet angles and comparison with similarity spectra of Tam et al. [21]. $M = 1.0, T_t/T_a = 3.2$. Symbols: solid lines: FSS data; dashed lines: LSS data.

The diameter of the jet is 2.45 in. Also shown in this figure are analytical spectral shapes, termed the fine-scale similarity spectrum (FSS) and large-scale similarity spectrum (LSS), extracted from data by Tam et al. [21]. The 1/3-octave peak frequency is at ~5000 Hz at 90 deg; the peak shifts to lower frequencies with increasing polar angle and occurs at ~1600 Hz at 150 deg. There are two schools of thought for the underlying reason: 1) in the traditional view, based on Lighthill's acoustic analogy and further extensions, convection amplification and mean flow/acoustic interactions are responsible for the observed differences, rather than an anisotropy inherent to the turbulent eddies, and 2) in the second viewpoint, propounded by Tam [22] among others, the large-scale turbulence structures in the jet flow directly radiate noise to large aft angles, and are far from being statistically symmetric, thereby providing a rich directivity. This phenomenon is especially present in jets with supersonic convective Mach numbers. This component of noise is generated at the periphery of the jet column, just outside the shear layer and as such is not subjected to mean flow/acoustics interaction or refraction effects. There is no general consensus on the physical mechanisms; regardless, the spectral shapes at angles close to the jet axis are distinctly different from those at the lower polar angles, as seen in Fig. 1.

Several theoretical formulations, which aim to predict the experimentally observed spectral characteristics of jet noise, have been proposed since the early 1970s. A review of all these approaches is given in Sec. III.B in [19]. The Doppler factor $[1 - M_c \cos(\xi)]$ figures prominently in all the traditional approaches which incorporate the notion of moving sources, both for normalizing the frequency and for calculating the effect of convective amplification on sound levels. M_c is the convective Mach number, usually taken to be ($\sim 0.7^* V_j/a$), where V_j is the jet velocity at the nozzle exit plane, (a) is the ambient speed of sound, and ξ is measured from the jet exhaust axis. With the experimental noise database, Viswanathan [20] examined the validity of the use of the Doppler factor and came up with some surprising conclusions. Figure 2, reproduced from [20], shows the normalized spectra at an inlet angle of 145 deg ($\xi = 35$ deg) plotted against the Strouhal number (fD/V_j, f is frequency in Hz and D is the jet diameter) without the Doppler correction. The jet Mach numbers (M) span a wide range of 0.3 to 1.0, and the jet stagnation temperature ratio (T_t/T_a) is 2.2. First of all, there is excellent collapse of the spectra for the higher Mach numbers over the entire frequency range; the lower Mach number spectra are obviously contaminated by rig noise, with the levels being higher by ~4 dB for the $M = 0.4$ jet over a wide range of higher frequencies. The level of contamination is much

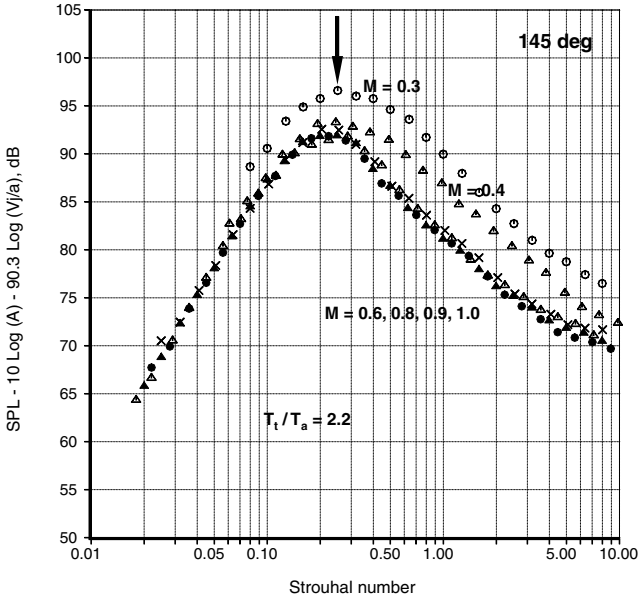

Fig. 2 Comparison of normalized spectra from heated jets. Data corrected to 20 ft (6.96 m). A is in square inches. $T_t/T_a = 2.2$, inlet angle = 145 deg. $M = 0.3$, 0.4, 0.6, 0.8, 0.9, and 1.0.

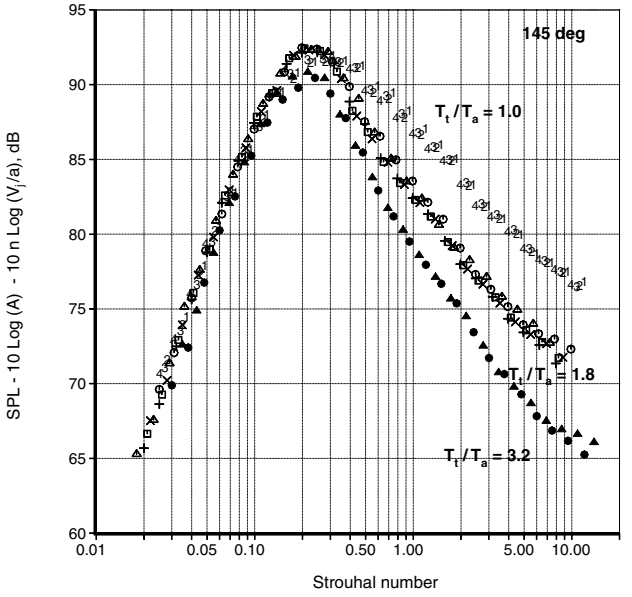

Fig. 3 Normalized spectra from jets at different velocities at 145 deg. Data corrected to 20 ft (6.96 m). Numbers: $T_t/T_a = 1.0$; open symbols: $T_t/T_a = 1.8$; closed symbols: $T_t/T_a = 3.2$.

higher for the $M = 0.3$ jet. (This issue of noise contamination at low Mach numbers has been dealt with in great detail in [18].) Let us examine the spectral shape and the alignment of the spectral peaks, while fully recognizing the effect of the rig noise on the elevated levels at the lowest two Mach numbers. It is clear that the spectral peaks are perfectly aligned at a Strouhal number of approximately 0.25, as denoted by the arrow in Fig. 2. The ratio between the Doppler factors (see Table 2 in [20]) for the lowest Mach number of 0.3 (0.753) and the highest Mach number of 1.0 (0.22) is 3.42. If we use the Doppler correction for the frequency ($f^*\{1 - M_c \cos(\xi)\}^* D/V_j$) on the x axis, the spectral peaks for these two Mach numbers will be spread apart by a factor of 3.42. Furthermore, each of the spectra at the other Mach numbers will be subjected to varying Doppler correction factors (0.662, 0.501, 0.358, and 0.283) and the perfect collapse and the alignment of the peaks will be completely destroyed.

Viswanathan [19] investigated the role of the term for convective amplification in trying to predict the different spectral shapes shown in Fig. 1. This term, as per Lighthill [1] and further extensions due to Ffowcs-Williams [23], is usually of the form:

$$D(\xi) = \left[(1 - M_c \cos\xi)^2 - \alpha^2 M_c^2\right]^{-5/2}$$

α is an empirical constant with a value of approximately 0.3. It has been established since the early 1970s that the theoretical directivity differs vastly from the experimental trends. A variety of adjustments to the above equation has been attempted to fit the data; these include combinations of different values for α and M_c, and a range of exponents from -3 to -9 (instead of -5). However, none of these approaches has provided satisfactory results even for the overall sound pressure level (OASPL) directivity, let alone the entire spectra. Scaling laws developed in [19] proved unambiguously that spectra from jets at different M but at a fixed stagnation temperature ratio can be collapsed at every radiation angle with a unique velocity exponent. Viswanathan [19] also found that the jet temperature ratio, rather than convective amplification, exerts a strong influence on the spectral shapes at the aft angles; see Sec. V in [19] for more details. A single figure is shown here to illustrate the trends. Normalized spectra at three temperature ratios of 1.0, 1.8, and 3.2 from jets at various M are shown in Fig. 3 at 145 deg. There are three distinct families of curves, each with a unique shape, at a particular jet temperature. The jet velocity at $M = 1.0$ and $T_t/T_a = 1.0$ ($V_j/a = 0.912$) is greater than the velocities for jets with 1) $M = 0.3$, 0.4, 0.5, 0.6, 0.7 and $T_t/T_a = 1.8$ ($V_j/a = 0.386$ to 0.9), and 2) $M = 0.3$, 0.4, 0.5 and $T_t/T_a = 3.2$ ($V_j/a = 0.516$ to 0.884). Yet, the spectral shapes have a narrower peak for the lower velocity jets at higher temperature in Figs. 3. Perfect collapse of the entire spectra without the Doppler factor has been demonstrated at various aft angles, from 110 to 160 deg, using the new scaling laws.

Note that the convective amplification term relies only on jet velocity (through M_c). Unless the temperature dependence is explicitly included in some fashion, there is no way this term can correctly predict the spectral shape at the aft angles. Thus, the inclusion of the Doppler factor, both for normalizing the frequency and for predicting the change in spectral shape, is seen to lead to poor results when judged against experimental data. Therefore, the first explanation is obviously too simple, as formulated. Another intriguing spectral trend is also highlighted: Viswanathan [18] showed that the spectral shape at a very low Mach number of 0.4 from unheated jets conforms to the LSS shape at large aft angles; see Fig. 19 and associated discussion in Sec. 4.3 in [18]. Note that the LSS shape was extracted from heated supersonic jets. It was hypothesized that the drastic collapse of the large-scale structures downstream of the potential core could be a possible mechanism.

III. Numerical Simulations

A. Objectives of Current Study

The above characteristics of jet noise from experiments set the stage for one of the objectives of the numerical simulations: is it possible to predict the change in spectral shape? There is strong experimental evidence which suggests that the contributions from the large-scale turbulence structures are important for noise radiation. LES is ideally suited for examining this issue. The unheated low Mach number (0.4) case provides a stringent test for assessing the ability of the LES methodology, as there is no obvious noise generation mechanism. This case is tackled first. There is strong Mach wave emission from highly heated jets at supersonic and high subsonic jet Mach numbers. That is, there is an identifiable source explained by the wavy-wall analogy, as opposed to the low velocity jets. Simulations are carried out for a perfectly expanded $M = 1.9$ jet and several heated subsonic jets from round nozzles. A heated underexpanded jet with strong shocks in the jet plume is also considered. Direct comparisons with the measured far-field noise are made for all the cases.

Steady-state RANS solutions, with a common turbulence model, provide only two quantities that describe the turbulence. There are two potential sources of error in noise predictions: inaccuracies in the computed flowfield and shortcomings in the noise models. It has generally been assumed that the principal reason for the poor

predictions was due to the inadequate computation/specification of the flow quantities which are then introduced into either Lighthill's or Lilley's [24] equations. Much of the effort so far has been directed at improving the flow predictions with better turbulence models, finer computational grids, etc. However, there is a fundamental problem with the acoustic models, which has not been recognized or well understood. As clearly demonstrated with concrete experimental evidence in Sec. II, all these approaches could be doomed to fail regardless of the quality of the computational fluid dynamics (CFD) solutions. Given the observations in Sec. II, perhaps it should not be surprising that all the current methods that use the RANS solutions as input to a noise solver based on the equations of either Lighthill [1] or Lilley [24] fail to predict the correct spectral shapes in the aft quadrant.

B. Description of the Methodology

Only a brief overview of the numerical procedure is provided here. A comprehensive description of the objectives of the numerical approach, a review of the state of the art and the pros and cons of the various choices/assumptions invoked by the different research groups, the rationale for the choice of the numerics, the reasons for selecting an integral method and not a direct method for noise computation, the grid topology, the effect of the location and shape of the FWH surface, the effect of the closing disk in the downstream direction, etc., are given in [13,14]. An extensive set of validation cases for testing and justifying each of the above choices is also provided in these two references. The issues of grid adequacy and grid-independent predictions up to a Strouhal number limit have also been addressed.

The turbulence is treated by LES and the Navier–Stokes equations are solved with a slightly upwind-biased high-order differencing for spatial discretization, and implicit time integration. The NTS code, described in [25], is run on structured multiblock curvilinear grids. The time integration is carried out with an implicit second-order scheme and dual time stepping. In the turbulent flow region and in the near field the spatial discretization uses a combination of fourth-order centered and fifth-ordered upwind-biased scheme, based on flux-difference splitting for the inviscid terms. Outside this region, purely upwind differencing is employed to damp out the outgoing waves. A buffer layer, in addition to nonreflecting boundary conditions, is included to ensure that reflections from the boundaries do not contaminate the solution in the domain of interest. For simulating the turbulence, the sub-grid-scale (SGS) model is deactivated, and the approach is viewed as "implicit LES." The slight dissipation introduced by the upwind scheme (with a typical weight of 0.25) serves the purpose of removing the energy that would be transferred to the unresolved scales as part of the energy cascade. Several other approaches were evaluated as well; this choice turned out to be the best option for simulating realistic spontaneous transition to turbulence without introducing any artificial forcing of the velocity profiles at the nozzle exit (at the inflow boundary of the LES domain), as explained in [13–15]. The realism of transition is judged visually; this is justifiable, keeping in mind that the details of the transition are not unique. We also note that experimental studies into the impact of boundary-layer thickness and even a laminar-or-turbulent state have failed to show a large impact, at least on the bulk of the noise for the nozzle geometries and test conditions considered here (see [26] for complete details). The initial conditions of the LES can be taken from a steady-state RANS solution or from an LES of the upstream flow. In the former case, three-dimensional random perturbations naturally develop very fast and therefore no artificial initial perturbations are needed. It is noted that sustained inflow forcing is not used in the simulations.

In a recent upgrade to the numerics, the ability to handle supersonic jets with shocks in the jet plume was improved, as described in [15]. A zonal method had been adopted in [13,14], where the order of the finite differencing was lowered from a fifth-order to a third-order scheme for the upwind differencing, and a flux limiter was activated in the regions where shocks were expected to form and assumed to be known a priori. This approach is not entirely satisfactory, because it is not possible to know where the shocks would be located for flows from complex geometries. A method for local automatic activation of the flux limiters was developed and tested for several jet Mach numbers from round and beveled nozzles by Shur et al. [15]; the adopted algorithm was robust and more accurate than the zonal method.

In the earlier computations, the nozzle geometry was not included. Rather, simple inflow conditions were specified at the inflow plane. When the beveled nozzles were first considered, it became clear that this approach would not suffice. The pressure distribution at the inclined nozzle exit plane is nonuniform, with strong gradients. These types of flow features, where the flow parameters are not uniform and there could be vectoring of the jet plume, preclude the manual specification of inflow conditions, and the flow inside the conical nozzle must be computed.

A large-eddy simulation of the entire flowfield, internal and external, is beyond the computational resources available to us and is not necessary for most aspects of noise prediction, because the noise is generated outside the nozzle. At practical Reynolds numbers, the computer requirements of a complete LES become prohibitive even for mainframe computers. Therefore, a two-step approach has been adopted. A RANS simulation is first carried out for the internal and external plume on a grid of approximately 2.2×10^6 points that provides an accurate resolution of the nozzle boundary layer. A LES is performed in a second step for the external plume on a grid which is coarser in the radial direction near the nozzle wall edge (resolving the viscous sublayer not being necessary), with the total pressure and temperature and the inflow velocity angles from the RANS simulation interpolated and specified as the inlet boundary condition. Note that as seen in Fig. 4, where typical velocity profiles are presented at the exits of the converging–diverging and converging (conical) nozzles considered below, both the shape of the profiles and corresponding boundary-layer thicknesses are rather different. For the convergent–divergent (CD) nozzle, the boundary-layer thickness defined by the level of 0.995 of the core velocity is $\sim 0.05D$ and for the converging nozzle the thickness (in this case it is defined by the position of the velocity maximum) is $\sim 0.008D$. The corresponding momentum thicknesses are $\sim 0.004D$ and $\sim 0.0005D$, respectively. Therefore, the value of the RANS resides not only in predicting inviscid effects such as slanting of the velocity profile due to streamline curvature, but also in boundary-layer properties. The inlet pressure for subsonic jets is calculated from a standard nonreflecting boundary condition. It has been verified that the time-averaged static-pressure field from the LES matches that from the complete RANS simulation, thus validating the two-step approach. The LES grids are more uniform than the RANS grids, stretching much more progressively in the streamwise direction, which is essential for simulations aimed at noise predictions. They have from approximately 1.5 to approximately 5×10^6 nodes, depending on the geometry and cycle conditions. The computational domain extends

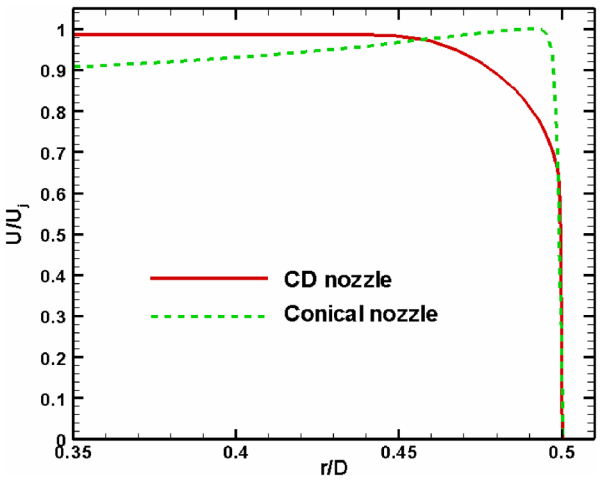

Fig. 4 Profiles of the streamwise velocity at the nozzle exit for the hot jets from converging conical and converging–diverging nozzles.

typically to $75D$ in the axial direction; in the radial direction, the grid extends to $17D$ upstream of the nozzle exit and progressively widens in the axial direction to accommodate the spreading jet, so that the half-width of the domain reaches up to ~40D at the last axial station.

The far-field noise is calculated through surface integrals, using the permeable FWH formulation. The FWH surface has a funnel shape and a closing disk at the downstream end. Because turbulence crosses this disk, the accuracy depends on a change of variables in the FWH equation. Several issues on the placement of the FWH surfaces, the use of the closing disks at the downstream end, the need to average over several (3–6) closing disks, etc., have been addressed in detail in [13,14]. Computations on multiblock structured grids are performed on personal computer clusters with up to six processors capable of 3.0 GHz each. Therefore, the number of grid points is lower than on mainframe machines. However, the resolved frequency range is not dramatically narrower, because of the chosen grid topology and the efficient distribution of the grid points. The highest resolved Strouhal number varies from approximately 1.5 to approximately 5 depending on the test case and the number of grid points. The highest Strouhal number is comparable or even higher than what is reached in the simulations carried out on supercomputers. Noise predictions from a variety of geometries and flow conditions such as single and dual-stream jets, jets with coflow, chevron nozzles, etc., have already been carried out and presented in [13–15].

IV. Results and Discussion

A. Effect of Grid Refinement

A grid refinement study was carried out to assess the impact of the grid density and grid distribution on both the flow and the noise. The case chosen was a heated jet with $M = 1.0$ and a stagnation temperature ratio (T_t/T_a) of 3.2. The coarser grid had a total number of grid points of approximately 1.5×10^6 for LES; the finer grid had approximately 2.7×10^6 points. It is known that the main noise producing regions of the jet are located just beyond the end of the potential core for low velocity jets. An additional expanded source of noise, due to Mach wave emission, is in the initial developing shear layer, starting close to the nozzle exit plane for convectively supersonic jets. To target this source, the new grid was significantly denser (by more than a factor of 2) in the axial direction, in the region of highest importance for noise. Additionally, the region with the fine grid was extended outward in the radial direction, enough to reach the FWH surface. This radial refinement had a most beneficial effect in that the resolved frequency (Strouhal number) range was extended considerably. In other words, the grid was refined not only in the simple sense of having more points, but also in terms of a more educated design. The time step was reduced from 0.03 to 0.02, normalized with diameter and jet velocity; on the other hand, the azimuthal spacing was unchanged.

Some specifics of the grids are provided. Different grids were used to meet the demands of the jet operating conditions. As noted later, all the grids are nonuniform in both the axial (x) and the radial (r) directions. In the x direction, the grid is clustered in the vicinity of the nozzle exit and is kept fine enough up to several diameters downstream of the jet potential core. In the r direction, the grids are clustered near the solid walls and in the shear layer. The azimuthal grid is uniform and has 72 cells in all the considered cases.

In the coarse grid used for the hot jets at $M = 0.6$ and $M = 1$, Δx varies from 0.03 at the nozzle exit up to 0.15 at the end of the potential core. The Δr value is 0.003 near the wall and grows to 0.025 in the middle of the shear layer at the x section corresponding to the end of the potential core. The Δr at the FWH surface varies from 0.04 up to 0.06, which provides a resolution of waves with $St \approx 2.5$ for $M = 0.6$ and ≈ 1.6 for $M = 1$, with the assumption that six cells per wavelength provide adequate resolution.

In the grid used for the $M = 0.4$ cold jet Δx varies from 0.007 at the nozzle exit up to 0.04 at the end of the potential core. The Δr is 0.0025 near the wall and grows to 0.02 in middle of the shear layer at the x section corresponding to the end of the potential core. The Δr at the FWH surface varies from 0.02 up to 0.08, which provides a resolution of waves with $St \approx 5.5$.

Table 1 Jet operating conditions

No.	Fully expanded Mach no.	T_t/T_a	Nozzle	Reynolds no.
1	0.6	3.2	Converging	2.5×10^5
2	1.0	3.2	Converging	4.2×10^5
3	1.56	3.2	Converging	8.5×10^5
4	0.4	1.0	Converging	5.7×10^5
5	0.9	1.0	Converging	1.2×10^5
6	1.92	2.7	CD	4.2×10^5
7	1.92	1.0	CD	2.8×10^5

Table 1 provides the details of the nozzle geometry, the jet conditions, and the Reynolds numbers for all the cases for which results are presented. It is noted that the Reynolds numbers in the simulations match those in the experiments.

Figures 5a and 5b show comparisons between the coarse and the fine-grid solutions. The variations of the time-averaged jet velocity, temperature, and the root-mean-square value of the axial velocity fluctuations along the jet centerline for the round jet are presented in Fig. 5a. The differences between the two sets of solutions are minor, with the length of the potential core predicted with the finer grid being $\sim 0.5D$ longer and a corresponding shift of the region of maximum turbulence intensity downstream of the end of the potential core. Figure 5b depicts the effect of the grid refinement on the shear layer turbulence. It reveals a sufficient drain of energy to the unresolved scales on both grids and an extended inertial range in the spectrum from the fine-grid simulation, which supports the credibility of the LES even with the deactivated SGS model. These results, taken together with earlier studies on grids, indicate that the grid with approximately 1.5×10^6 nodes is fully adequate for computations of both the mean flow and the turbulent statistics, at least along the centerline. Experience then allows us to determine the reliable region of the predicted spectra, primarily based on unnaturally steep drops or spurious peaks.

In spite of the marginal effect of the grid refinement on the mean solution on the centerline, the alteration of the predicted noise characteristics due to the grid refinement turned out to be quite significant. There are noticeable differences between the two sets of solutions when the instantaneous vorticity and pressure–time derivative fields are examined in Fig. 6. The fine-grid simulations reveal a lot more fine-scale activity (Figs. 6a and 6b) and consequently higher levels of high-frequency noise. Further, as seen in Figs. 6c and 6d, there is a clear increase in the low-frequency noise radiated to the peak radiation sector in the aft quadrant, and a downstream shift of the peak radiation angle by ~5 deg for this case. Figure 7 shows comparisons of the sound spectra obtained with the two grids at polar angles of 50, 80, 130, and 140 deg with measured data from [16]. The spectra have been corrected to a polar arc of 20 ft (6.96 m) with the coordinate system centered on the jet axis on the nozzle exit plane, and to standard-day ambient conditions (77°F and 70% relative humidity). Note that the computed spectra display tail-up at the high-frequency end, and more so with the coarse grid. They are probably related to the excessively two-dimensional character of the transition to mixing-layer turbulence, which causes a nonphysical tone in the sound spectra. Its frequency grows and its amplitude drops with grid refinement (this issue is discussed in detail in [13]). Vigorous three dimensionality can be induced artificially, but arbitrary parameters enter the simulation, and the realism of the early turbulence is still judged visually. Considering this, the overall sound intensity is computed by integration of the spectra from zero up the last $1/3$ octave not containing any tone. Depending on the grid, this corresponds to a Strouhal number from 1.35 (the coarse grid) up to 5.0 (for the finest grid used for the simulation of the cold $M = 0.4$ jet considered below). An examination of Fig. 7 indicates that there is a drastic improvement in the predicted spectral shapes with the fine grid, and the highest resolved frequency reaches ~25 KHz. There is almost a doubling of the range of well-predicted Strouhal numbers, from approximately 1.35–2.7; the predicted peak levels are also approximately 3 dB higher at the aft angles, thereby moving them closer to data. The predicted and measured directivities

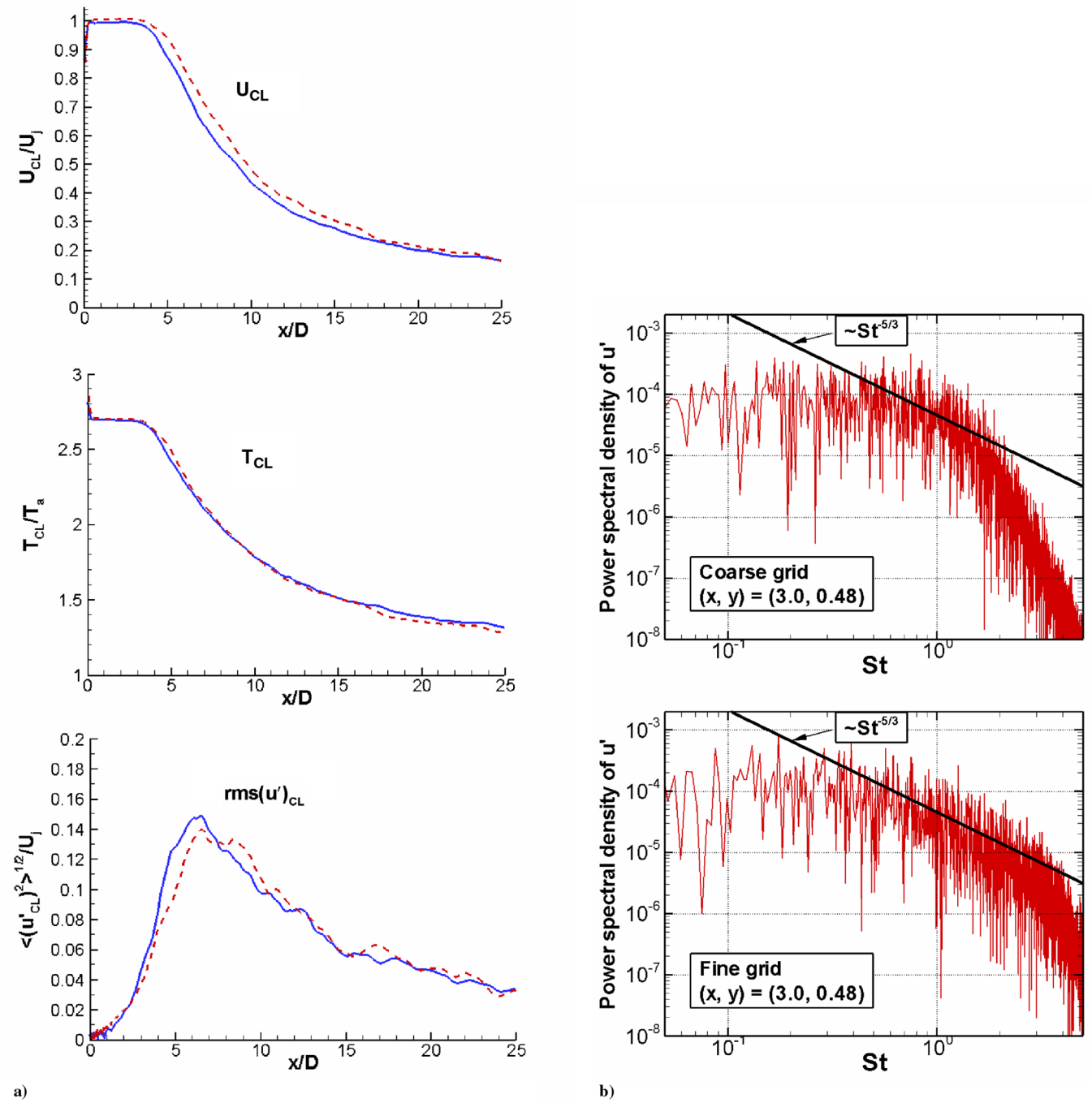

Fig. 5 a) Comparisons of solutions obtained with coarse and fine grids. $M = 1.0$, $T_t/T_a = 3.2$. Top: centerline velocity; middle: centerline temperature; bottom: root-mean-square value of axial velocity fluctuations. Solid lines: coarse grids; dashed lines: fine grids. b) Power spectral density of the axial velocity fluctuation in the shear layer. $M = 1.0$, $T_t/T_a = 3.2$.

of the OASPL are shown in Fig. 8. The main improvement is in the peak radiation sector; though there still is underprediction when compared with data, the magnitude of the discrepancy is now only approximately 2–3 dB. The most significant improvement is that the predicted peak angle matches the measured one, whereas it is off by approximately 10 deg for the coarser grid. Similar improvements to noise are also seen for beveled nozzles (not shown). Based only on the mean flow and the turbulence statistics from time-averaged LES solutions, as shown in Fig. 5a, one would not expect such a major spectral and directivity effect of grid on noise. This example points to the importance of resolving the subtleties of the flow features responsible for noise generation and radiation and adds to the evidence against the ultimate potential of RANS-based approaches to jet noise prediction.

B. Investigation of Noise Sources

1. Experimental Data for Verification of Source Locations

Several types of comparisons between experiment and numerical simulations are shown, including the axial variations of the mean flow and turbulent fluctuations, far-field spectra, and source locations. A brief description of the source measurements is first provided, and detailed discussions will be presented in an upcoming paper by Viswanathan [27]. A directional microphone system consisting of an elliptic mirror is used to investigate the sources of noise in jets operated at subsonic and supersonic Mach numbers, both at unheated and heated conditions. The principle of the elliptic mirror system is first reviewed. Figure 9 shows a schematic of the elliptic mirror. The microphone is located at the near focus and the source of interest at the far focus. For applications to jet noise, the far

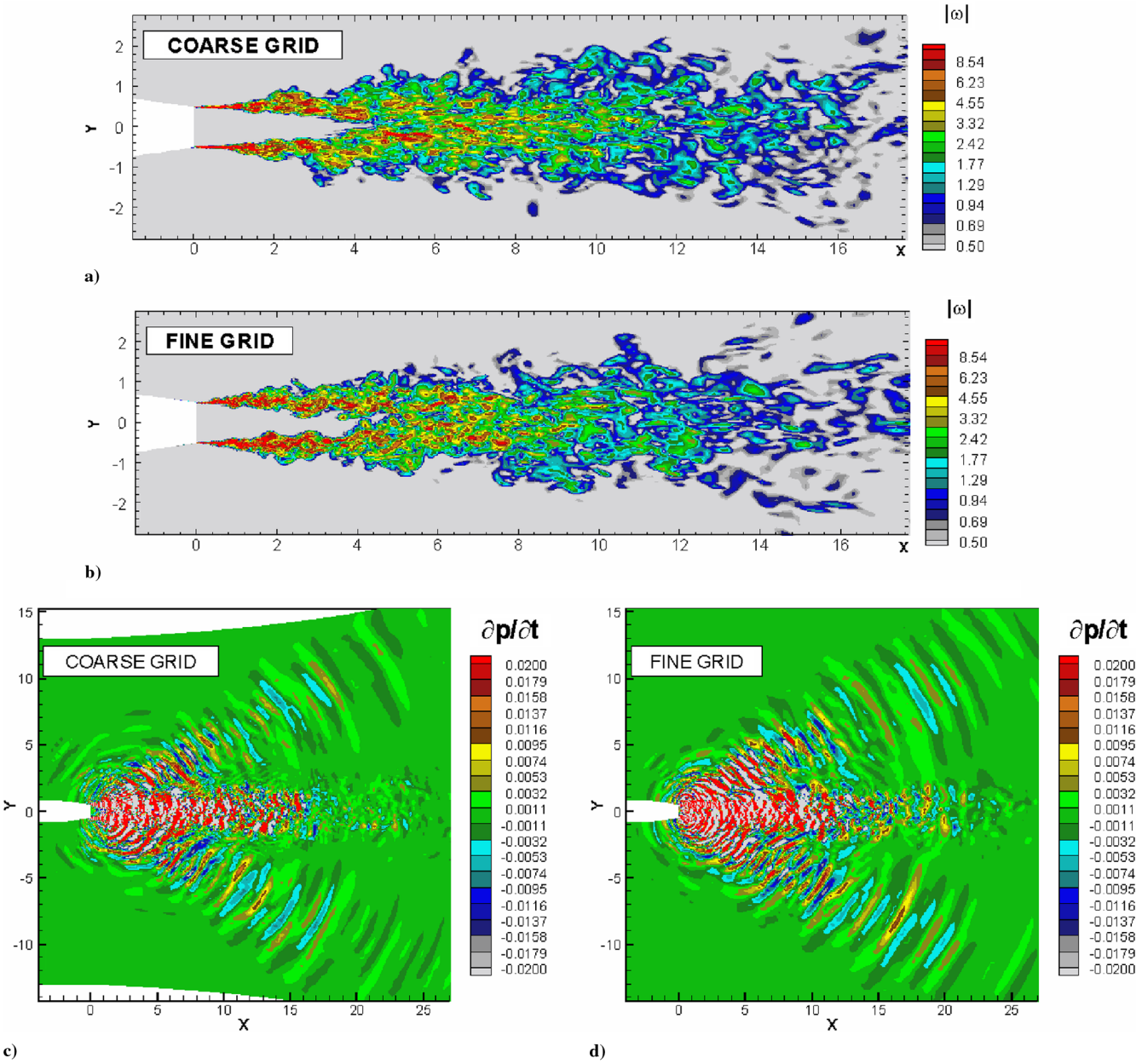

Fig. 6 Comparisons of solutions obtained with coarse and fine grids. $M = 1.0, T_t/T_a = 3.2$. a), b): instantaneous vorticity contours; c), d): instantaneous pressure–time derivative, normalized with ambient speed of sound, density, and D.

focus is typically located on the jet centerline. Consider a point source, denoted by the star, which is located offaxis from the major axis of the mirror. The combined path length ($L1 + L2$) controls the relative phase between the acoustic rays arriving at the microphone via different parts of the mirror. When the source is at the far focus, the combined distance ($L1 + L2$) is constant and the microphone senses a strong signal. However, when the source is displaced transversely from the major axis of the mirror, the path lengths begin to vary and there is destructive interference, resulting in a drop in the strength of the sensed signal. Thus, the mirror has the desirable property of distinguishing between sources that are located on the far focus from those that are displaced in the transverse or lateral directions. It should be kept in mind though that the resolution is not a sharp point but a small region near the far focus. The spatial resolution is a strong function of the source frequency; higher frequencies are better resolved because the same difference in the path lengths results in a larger phase difference. The reduced resolution of the lower frequency waves is a problem associated with all microphone array techniques as well.

It should be clear from the foregoing discussion that it is critical to locate the far focus of the mirror on the jet centerline. Typically, the mirror viewing angle (also referred to as look angle hereafter) is normal to the jet axis and the mirror is traversed parallel to the jet axis, mapping the source strengths along the jet column. However, when the source distributions at different view angles are desired, the requirement of always maintaining the far focus on the jet centerline imposes a burden on the design of the traversing mechanism and represents a serious engineering challenge. Detailed explanation is provided in [27] on how this requirement is met. It is simply noted that the noise sources have been mapped from various look angles, ranging from 90 to 150 deg for a variety of test conditions considered in the numerical simulations. The experimental measurements are included for comparison with the LES predictions at the appropriate sections of the paper.

2. *Low Velocity Jets*

The flow and noise of the $M = 0.4$ unheated jet are first examined. Given the difficulties with predicting noise at low jet velocities (due to the high power of Mach number that governs the acoustic efficiency), the number of grid points has been increased to approximately 3.5×10^6. Figure 10 shows comparisons of the computed time-averaged LES results with the laser Doppler

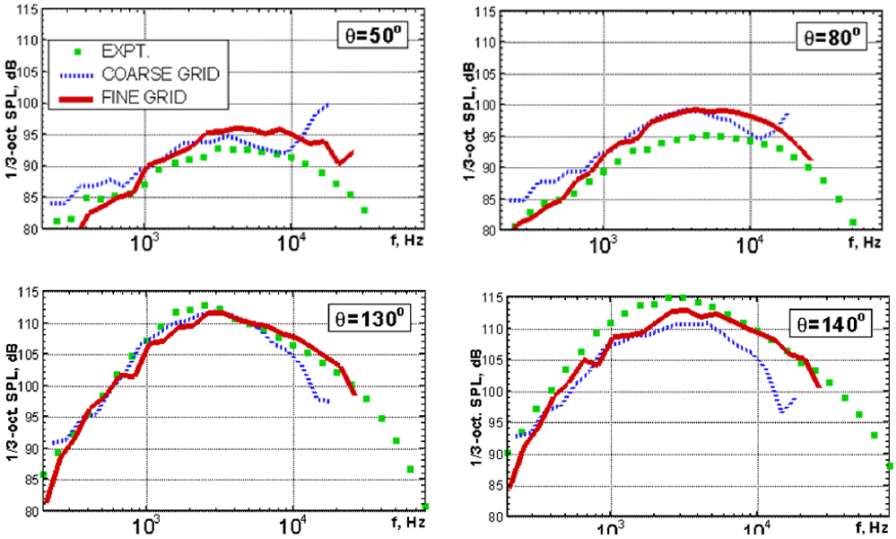

Fig. 7 Comparisons of spectra obtained using coarse and fine grids with data. $M = 1.0$, $T_t/T_a = 3.2$. Symbols: experiments; solid lines: fine-grid predictions; dashed lines: coarse grid predictions.

velocimetry (LDV) measurements of Lau et al. [28] and Lau [29] for an unheated jet at a Mach number of 0.28. The slightly lower Mach number in the experiments would yield a shorter potential length (by $\sim 0.1D$) as per the correlation formula developed from the experimental data. The variations of the mean axial velocity and the root-mean-square values of the axial and the radial fluctuating velocities are presented in Fig. 10. The end of the potential core is at $\sim 4.5D$, which is close to the experimentally measured value. The decay of the mean velocity with downstream distance is also in good agreement. In Fig. 10b, the peak level of the axial fluctuation velocity occurs at $\sim 8D$ and reaches 14%. In Fig. 10c, the peak predicted level of the radial fluctuation velocity occurs at $\sim 7D$ and reaches approximately 11%. As seen, there is good agreement between the predicted and measured turbulence statistics on the jet centerline. Comparable agreement of the turbulence in the shear layer is seen in Fig. 11; LDV data at two jet Mach numbers of 0.28 and 0.9 are included. In addition to the axial and radial turbulence intensities, the predicted shear stress levels are also close to the experimental data. Note that there is no data in the initial shear layer, the first data point being at $\sim 2D$, which precludes a comparison precisely where LES has a somewhat unexpected behavior. It is therefore not clear if the predicted spike close to the nozzle exit is accurate or is an artifact of inadequate resolution of the initial shear layer transition.

Figure 12 shows a comparison of the OASPL directivity with data. The reasonable agreement with the absolute levels and the good agreement with the trend of increasing noise levels with inlet angle give us confidence that the right physics is captured in the LES.

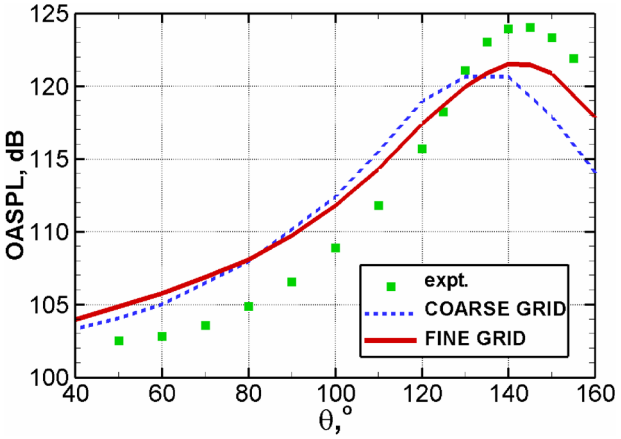

Fig. 8 Comparisons of OASPL directivity computed using coarse and fine grids with data. Data corrected to 20 ft (6.96 m). $M = 1.0$, $T_t/T_a = 3.2$.

Spectral comparisons with measured data are provided at various polar angles of 70, 120, 130, and 140 deg in Fig. 13a. The spectra at large aft angles of 150, 155, and 160 deg are shown separately in Fig. 13b; note the spectral shapes seen in Figs. 13a and 13b. For this low velocity jet, the spectral shape conforms to the FSS shape in the angular sector of 50 to approximately 140 deg. Further aft, the measured spectral shape has a sharper peak and has the LSS shape. The predicted spectra also have this narrower peak and there is a clear change from the shapes at lower angles. That is, the LES is able to predict this trend for this low velocity jet.

The variations of the axial source distributions as measured by the elliptic mirror, both the overall levels as well as for fixed Strouhal numbers, with the normalized axial distance (x/D) are presented in [27]. Figure 14 shows the variation of OASPL, for the unheated jet with $M = 0.4$ from several look angles. The peak source regions for all the view angles are located at a distance of $\sim 5D$ to $\sim 7D$ for the $M = 0.4$ jet. Note that the length of the potential core for this low velocity jet is $\sim 4.5D$, as seen in Fig. 10.

To get insights to the noise source mechanisms from LES, a movie has been made from the LES results. This movie clearly shows two noise sources. A snapshot of the vorticity and the pressure-time derivative ($\partial p/\partial t$) fields is shown in Fig. 15. This quantity is normalized by ($\rho_\infty a^3/D$), the ambient values of density and the speed of sound and the jet diameter (D). The vorticity contours and the movie depict visually some typical jet-flow turbulence features. In particular, they indicate the early shear layer roll up, vortex pairing, and the flow subsequently becoming chaotic with the formation of larger and larger vortical structures in the course of the shear layer evolution. These vortices reach the size of the nozzle diameter in the vicinity of the end of the potential core of the jet. The

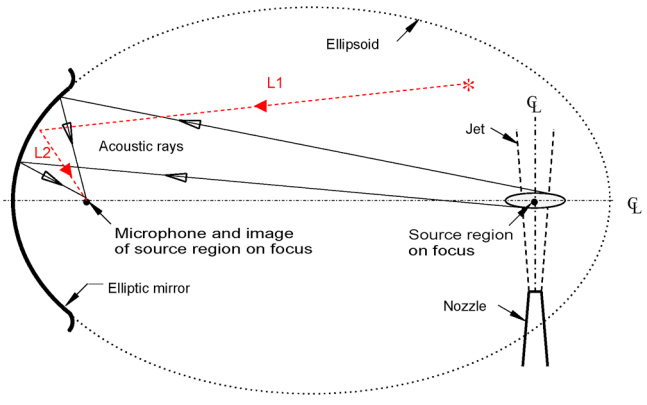

Fig. 9 Schematic of the elliptic mirror and its operating principle.

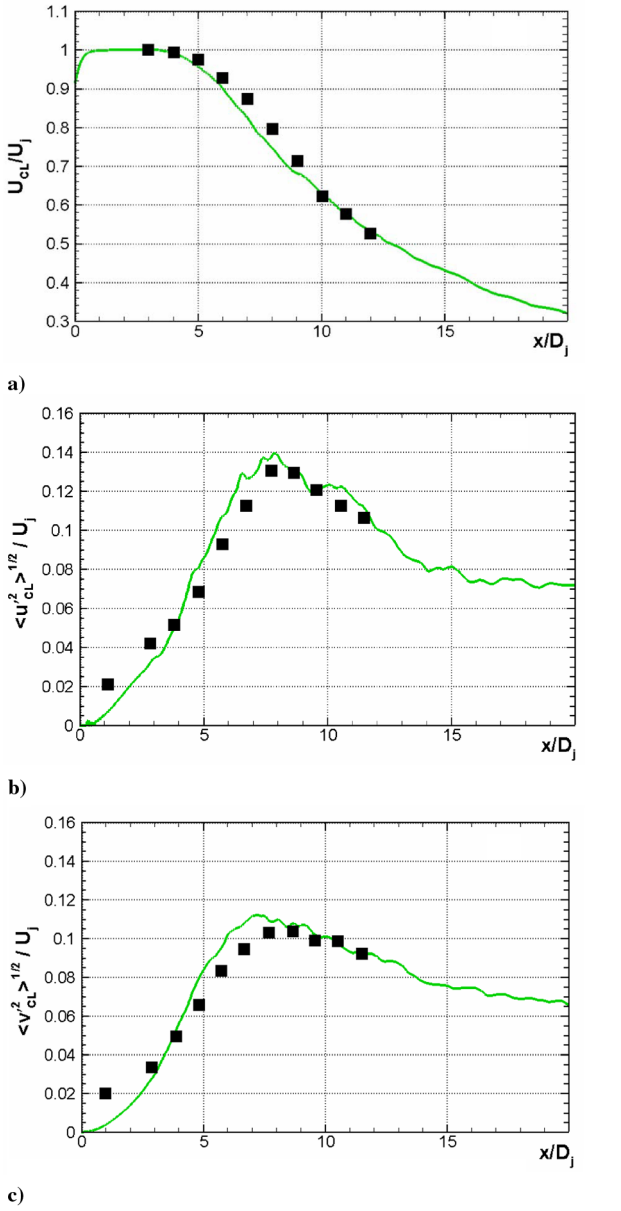

Fig. 10 Axial variations on the jet centerline. $M = 0.4$, $T_t/T_a = 1.0$. Symbols: experiments; lines: predictions. a) centerline velocity; b) root-mean-square value of axial velocity fluctuations; c) root-mean-square value of radial velocity fluctuations.

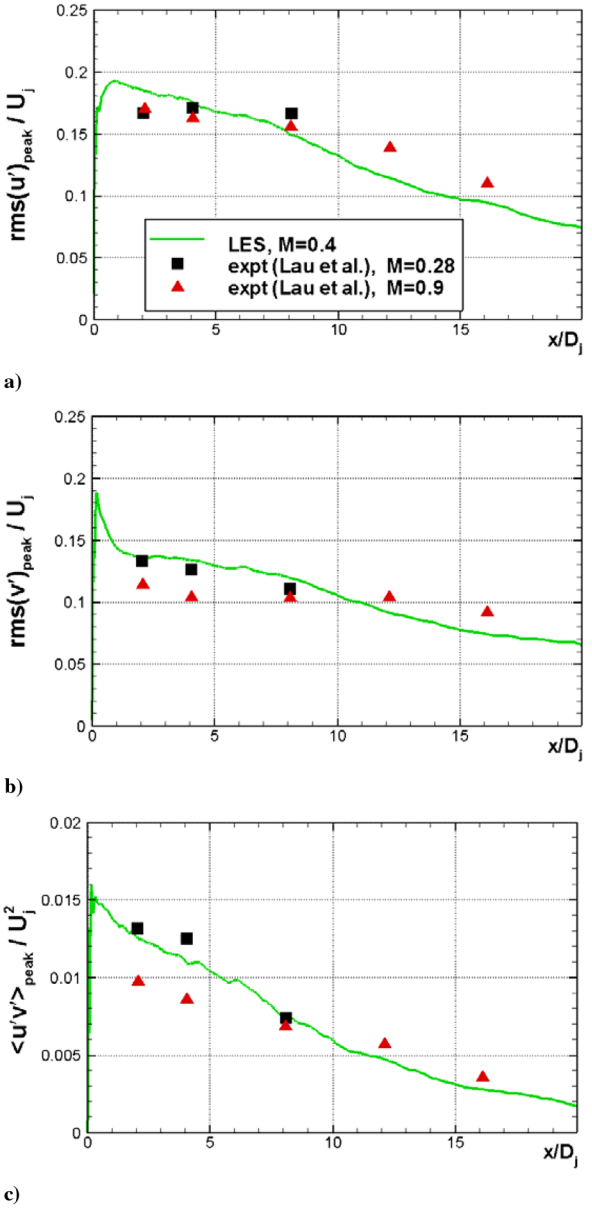

Fig. 11 Axial variations in the shear layer. $M = 0.4$, $T_t/T_a = 1.0$. Symbols: experiments; lines: predictions. a) root-mean-square value of axial velocity fluctuations; b) root-mean-square value of radial velocity fluctuations; c) Reynolds shear stress.

collapse of these structures, which occurs farther downstream, is probably responsible for the strong noise source that is known from correlation and elliptical-mirror measurements to be present between about $5D$ and $10D$. The $(\partial p/\partial t)$ plot appears to reveal a local source at a downstream distance of $\sim 7.5D$, with identifiable acoustic waves beamed to large aft angles. In addition, one can see concentric waves also radiated to lower polar angles from this source (these are much clearer in the movie). Extensive numerical verifications will determine whether this source is fully physical. The second noise source revealed by the $(\partial p/\partial t)$ plot is located in the shear layers close to the nozzle exit; the acoustic waves from this source are almost omnidirectional, and there is no directional radiation as with the source at $\sim 7.5D$.

The flow and noise for a higher velocity case, an unheated $M = 0.9$ jet, are now presented. The number of grid points is further increased to approximately 5.5×10^6 so as to push the predicted Strouhal number range higher, to approximately 5. The variations of the mean flow and turbulence properties along the jet centerline are presented in Fig. 16. In addition to the LDV data of Lau et al. [28,29], data from more recent measurements using particle image velocimetry (PIV) from Arakeri et al. [30] for the axial turbulence intensity are also included in Fig. 16b. The decay of the mean axial velocity is in excellent agreement with the data in Fig. 16a, where the potential core length is $\sim 5.5D$. We also note that the two sets of measurements, with different experimental techniques, are very

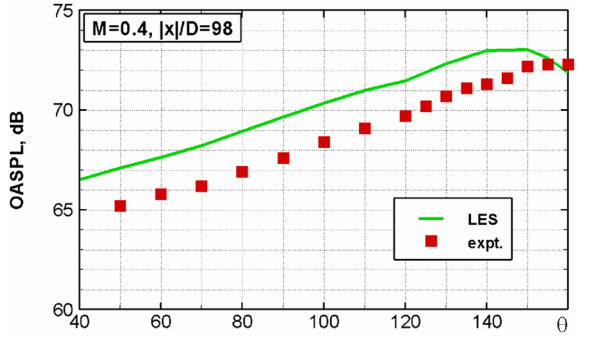

Fig. 12 Comparison of predicted and measured OASPL directivity. $M = 0.4$, $T_t/T_a = 1.0$. Symbols: experiment; line: prediction.

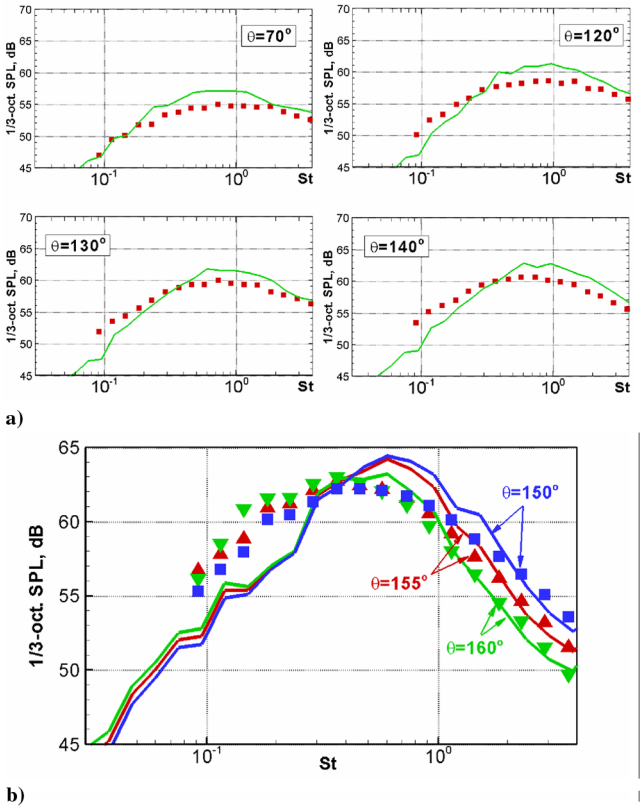

Fig. 13 Comparison of predicted and measured spectra. $M = 0.4$, $T_t/T_a = 1.0$. Symbols: experiments; lines: predictions. a) lower angles, broad spectra; b) aft angles, narrow peak.

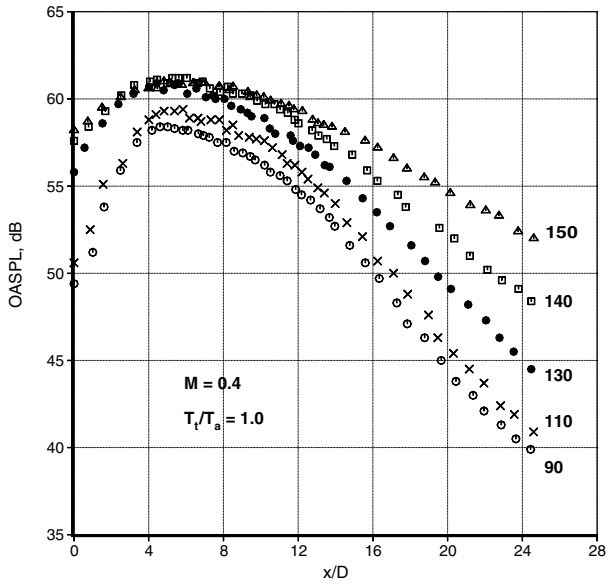

Fig. 14 Typical source distributions for various radiation angles. $M = 0.4$, $T_t/T_a = 1.0$.

close to each other on the jet centerline, and the prediction is again good. However, the predicted peak radial turbulence intensity in Fig. 16c is about 20% higher than the measurements.

The variations in the shear layer are compared with the two sets of data in Fig. 17. First of all, there are significant differences between the two sets of data in the shear layer, in contrast with the centerline situation. In general, the PIV values are substantially lower in the initial shear layer and up to an axial distance of $\sim 5D$. Whereas the PIV data show a gradual increase starting at a low value, the LDV data have the opposite trend of a gradual decrease and a high initial value close to the nozzle exit. There could be potential problems with resolution in the PIV measurements in the very thin initial shear

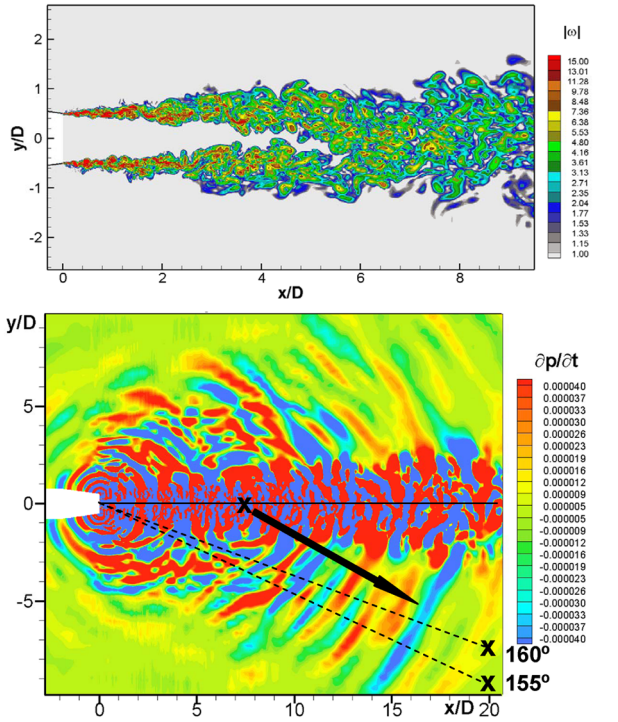

Fig. 15 Instantaneous contours of vorticity (top) and pressure–time derivative (bottom). $M = 0.4$, $T_t/T_a = 1.0$.

layer; it is not clear what the true distributions might be in the very early shear layer (in transition from a boundary layer) where the LES predicts sharp peaks. Anyhow, there is good agreement between the predictions and the LDV data in the region $x \geq 2D$.

Spectral predictions and comparisons with data are shown in Fig. 18 at four radiation angles of 90, 120, 140, and 150 deg. The predicted spectra are close to the data up to a Strouhal number of approximately 5 at all the angles. The change in spectral shape with angle is again captured accurately in the simulations. Thus, the flow and noise predictions for this jet, with the largest grid so far, are in favorable agreement with data.

Next we consider the case of the $M = 0.6$ heated jet with a jet stagnation temperature ratio of 3.2. Figure 19 shows spectral comparisons for this jet condition. For this case, only the coarse grid ($\sim 1.5M$ nodes) results are available. The maximum meaningful Strouhal number is approximately 1.5 (this corresponds to a model-scale frequency of 8600 Hz). The tail-up around this frequency is caused by numerics resulting in an excessively two-dimensional transition process; recall that this problem has since been eliminated (along with a fine grid) in Fig. 7 for the $M = 1.0$ jet at the same temperature. Apart from this, there is good agreement with the data. Further, the change in spectral shape from the broad to narrow peak is well captured in the LES. Discussions on the significance of these results are deferred till the LES results for other Mach numbers are presented.

3. *Higher Velocity Jets*

The noise characteristics of a perfectly expanded $M = 1.9$ jet at two temperature ratios of 1.0 and 2.7 are examined. The OASPL directivities are first shown in Fig. 20. In the experiments, the peak radiation direction is at approximately 150 deg for the unheated case and at approximately 125 deg for the heated case. The LES results correctly predict the shift in the peak radiation angle by approximately 20–25 deg, when the jet is heated. Further, the absolute levels are also predicted quite well for the heated jets. Figures 21 and 22 show spectral comparisons at a variety of polar angles for the unheated and heated cases, respectively. There is very good agreement for all the angles; note that the highest resolved model-scale frequency is approximately 40 KHz for these two cases.

The source measurements with the elliptic mirror for the unheated jet with $M = 1.9$ are shown in Fig. 23. There are two distinct sources:

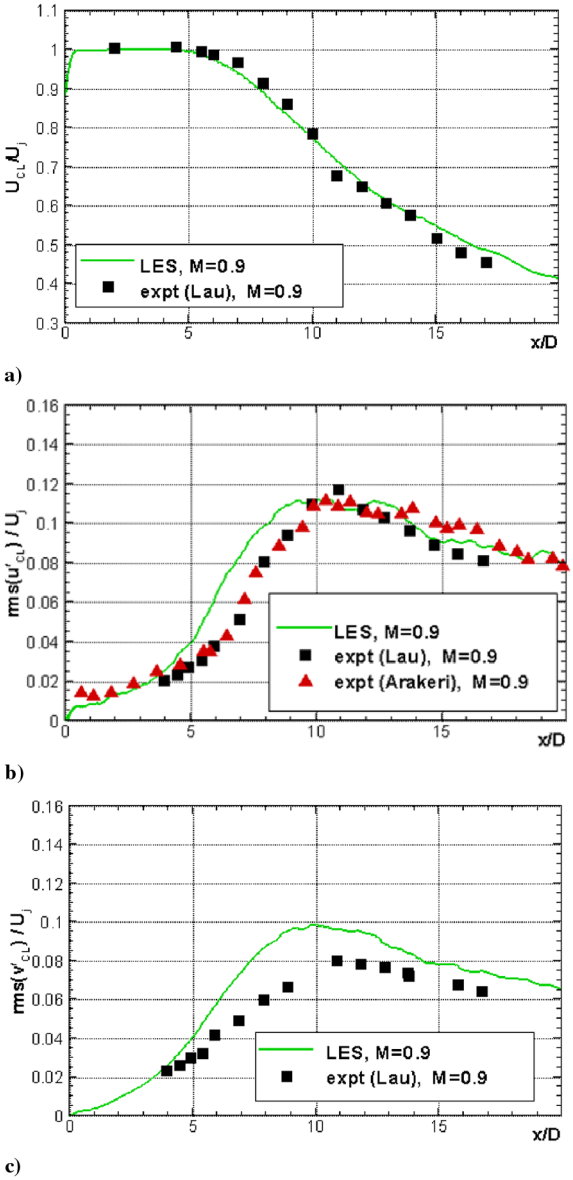

Fig. 16 Axial variations on the jet centerline. $M = 0.4$, $T_t/T_a = 1.0$. Symbols: experiments; lines: predictions. a) centerline velocity; b) root-mean-square value of axial velocity fluctuations; c) root-mean-square value of radial velocity fluctuations.

one is at $\sim 16D$ which radiates to the lower angles. The peak source location for the aft angles is much closer to the nozzle exit plane, at $\sim 8D$. Recall that for this high supersonic jet Mach number there is intense directional Mach wave radiation in the aft direction. Figure 24 shows instantaneous pressure–time derivative fields for the jets at the two temperature ratios. The Mach wave radiation associated with these supersonic jets is evident. The origin of this noise source is in the shear layer, within the first few diameters from the nozzle exit. A second source is located on the jet axis at a distance of $\sim 14D$. Thus, there are two strong sources for these jets, one on the jet centerline (as for the low velocity jet) and another one in the initial shear layer. These two sources may be identified more easily in the movies. Note further that the peak radiation angle for the Mach wave radiation moves to a lower polar angle for the heated $M = 1.9$ jet. The peak emission angles are close to the Mach angles given by the relation $[\cos^{-1}(1/M_c)]$. For the heated jet, the value of the Mach angle is 54.7 deg (assuming $0.7V_j/a$ for M_c), which corresponds to an inlet angle of 125 deg, that is, exactly the peak emission angle, as seen in Fig. 20. Clearly, the predicted source locations are in very good agreement with the source measurements with the elliptic mirror.

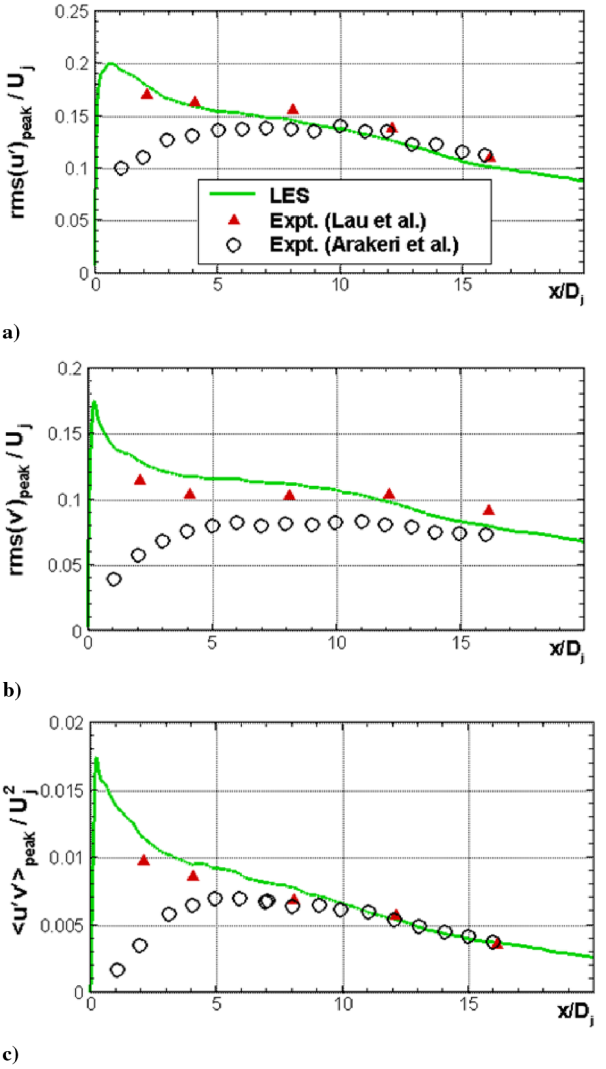

Fig. 17 Axial variations in the shear layer. $M = 0.9$, $T_t/T_a = 1.0$. Symbols: experiments; lines: predictions. a) root-mean-square value of axial velocity fluctuations; b) root-mean-square value of radial velocity fluctuations; c) Reynolds shear stress.

We briefly reexamine the results already presented for the $M = 1.0$ jet with $T_t/T_a = 3.2$ in Sec. IV.A. There is strong Mach wave radiation in Fig. 6d; the convective Mach number for this highly heated subsonic jet is 1.15, which is supersonic with respect to the ambient speed of sound. Therefore, one would expect Mach wave radiation. Elliptic mirror measurements for a comparable case of $M = 0.9$ and $T_t/T_a = 3.2$ are shown in Fig. 25. The convective

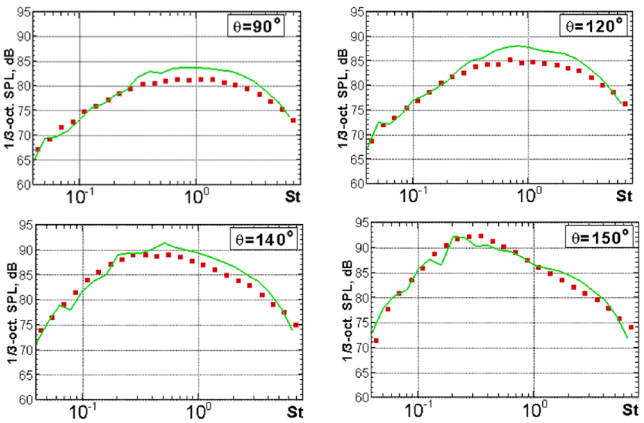

Fig. 18 Spectral comparisons, $M = 0.9$, $T_t/T_a = 1.0$. Symbols: experiments; lines: LES.

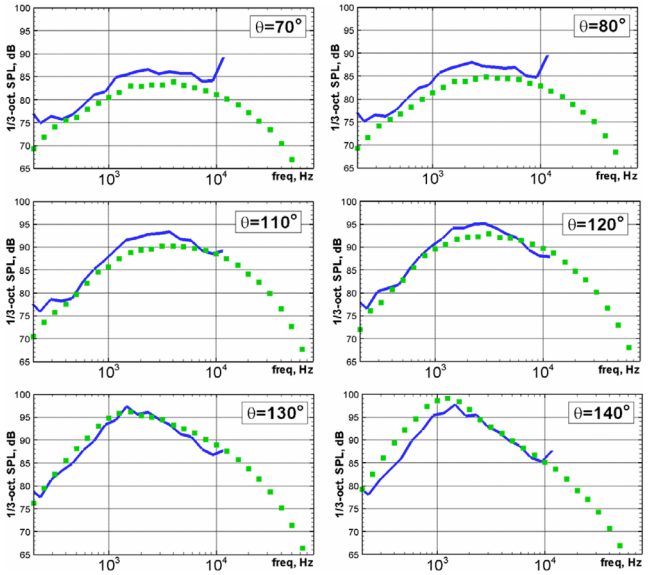

Fig. 19 Comparison of predicted spectra with data. $M = 0.6$, $T_t/T_a = 3.2$. Symbols: data; lines: predictions.

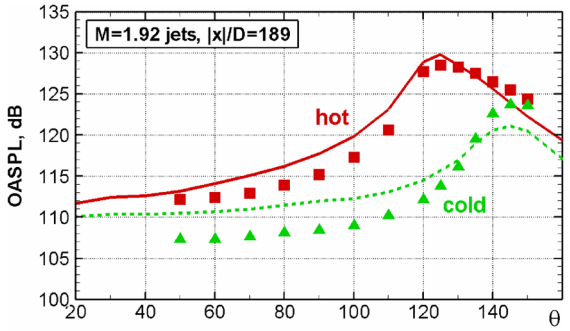

Fig. 20 Comparison of predicted and measured OASPL directivity. Squares, solid line: $M = 1.9$, $T_t/T_a = 2.7$; triangles, dashed line: $M = 1.9$, $T_t/T_a = 1.0$. Symbols: experiments; lines: predictions.

Mach number is again supersonic, with the resultant Mach wave radiation. As seen for the supersonic jet in Fig. 23, the mirror measurements show two distinct sources, one downstream of the potential core at $\sim 8D$ and one in the initial shear layer closer to the nozzle exit. However, note that the lengths of the potential cores are substantially different for the $M = 0.9$ heated jet and the unheated $M = 1.9$ jet. The spectral shapes shown in Fig. 7 have the FSS shape at the lower two polar angles, gradually change shape, and have the LSS shapes for radiation angles ≥ 140 deg as seen in Fig. 1. It is obvious that the LES correctly captures these experimental trends over a wide range of M_c, from $\cong 0.28$ for the unheated $M = 0.4$ jet, to $\cong 1.73$ for the heated $M = 1.9$ jet with a temperature ratio of 2.7.

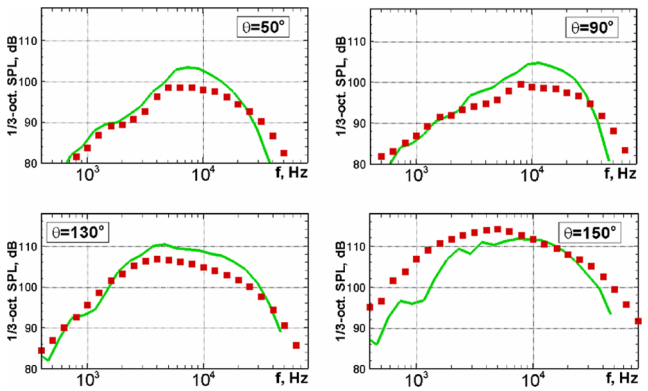

Fig. 21 Comparison of predicted and measured spectra at various polar angles. $M = 1.9$, $T_t/T_a = 1.0$. Symbols: experiments; lines: predictions.

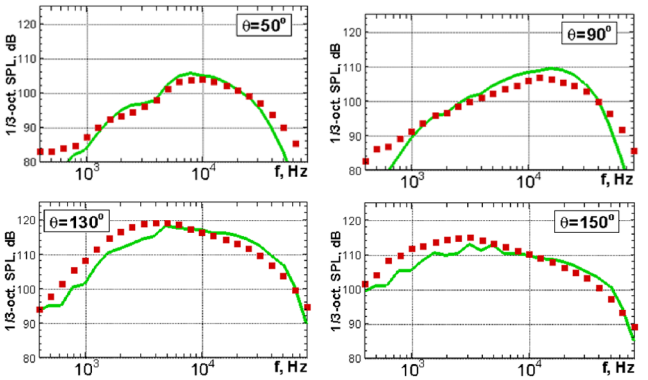

Fig. 22 Comparison of predicted and measured spectra at various polar angles. $M = 1.9$, $T_t/T_a = 2.7$. Symbols: experiments; lines: predictions.

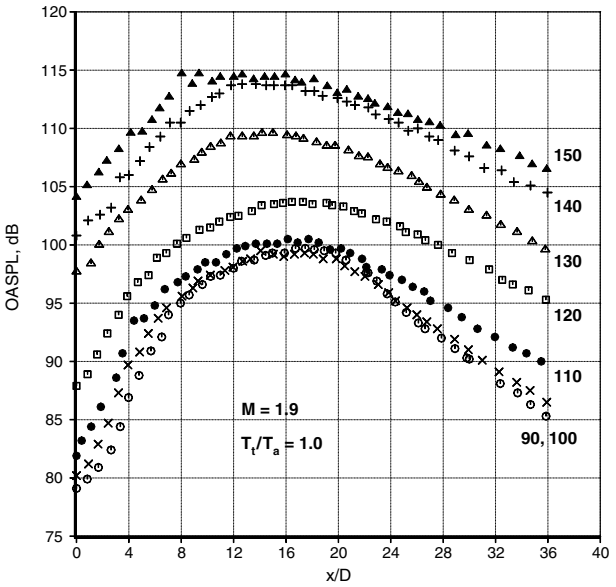

Fig. 23 Typical source distributions for various radiation angles. $M = 1.9$, $T_t/T_a = 1.0$.

The corresponding jet velocities span a range of 440 ft/s (134 m/s) to 2770 ft/s (845 m/s) and the increase in noise level for this range of jet velocity is very wide: ~ 63 dB. Note that the absolute predictions are usually within ~ 3 dB for this wide velocity range, without any empirical constants whatsoever in either the flow or noise computations.

4. *Discussion of Noise Sources*

Several theories have been proposed on the nature of the noise sources since the pioneering work of Lighthill [1]. The many approaches based on the classical theories of jet noise are described in great detail by Lilley [31]. As noted in Sec. II, these theories do not take account of the large-scale structures, and, in particular, their inherent anisotropy. The importance of the large-scale turbulence structures in the noise radiation of high-speed jets has been recognized since the early 1970s. Hot-wire measurements of the flow and acoustic measurements in both the near field and far field by McLaughlin et al. [32,33] provided substantial evidence that the large-scale structures are responsible for the generation of noise in high-speed jets. For supersonic jets, and subsonic jets at high temperatures as in practical jet engine applications, the large-scale structures propagate downstream at supersonic speeds relative to the ambient speed of sound. The review article by Tam [22] provides a detailed description of the physical mechanism by which supersonically propagating large-scale structures/instability waves generate noise. These structures are efficient generators of noise and constitute the dominant noise sources, especially in the downstream direction. At lower polar angles, the spectral characteristics are very

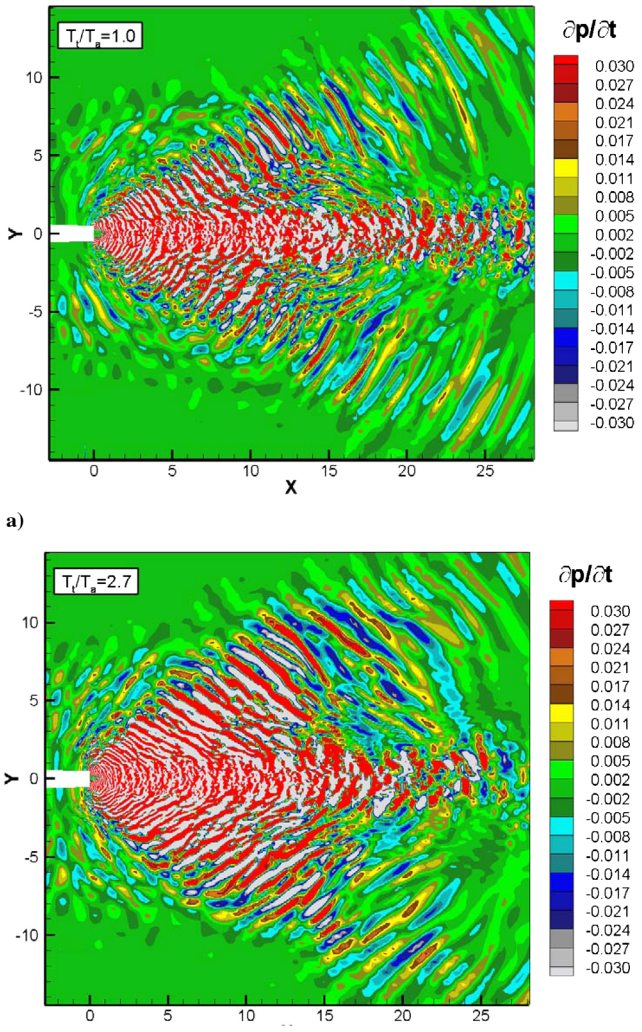

Fig. 24 Instantaneous field of pressure–time derivative. $M = 1.9$. a) $T_t/T_a = 1.0$; b) $T_t/T_a = 2.7$.

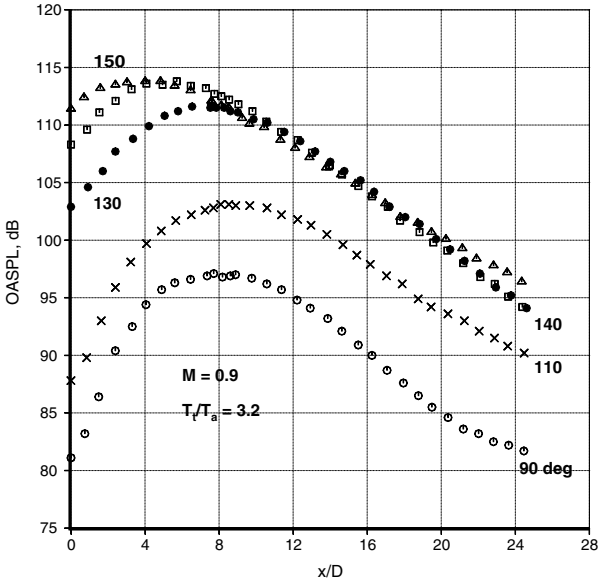

Fig. 25 Typical source distributions for various radiation angles. $M = 0.9$; $T_t/T_a = 3.2$.

different. Based on the experimental data, it has been proposed in [18,21] that there are two independent noise components, with the noise from the fine-scale turbulence being dominant at the lower angles.

Recently, Panda and Seasholtz [34] and Panda et al. [35] have carried out detailed correlation measurements of the flow fluctuations at various points in the jet column with the far-field pressure. A nonintrusive diagnostic technique based on Rayleigh scattering was used to measure the fluctuating quantities inside the jet. Correlations between points on the lip line (shear layer) or on the jet centerline with the noise signature at various radiation angles were obtained for a wide range of jet Mach numbers of 0.6 to 1.8. The main findings of these measurements are summarized here. For the far-field microphone located at an angle close to the jet axis (150 deg), significant correlation was measured from the peripheral shear layer for flows with supersonic convective Mach numbers; there was no such correlation for subsonic convective Mach numbers. Strong correlations at low Strouhal numbers were observed with the fluctuations along the jet centerline downstream of the potential core for all jet velocities. The highest correlation levels were always observed at large aft angles. As the microphone was moved to a lower polar angle of 120 deg, there was a sharp decrease in the correlation levels. For example, the correlation coefficient dropped from 0.17 at 150 deg to 0.02 at 120 deg for an $M = 1.4$ unheated jet; at still lower angles, the correlations were below the experimental noise floor. At lower polar angles, there was no measurable correlation with any location in the jet, for any Mach number. These studies established that 1) the fluctuations from the large coherent structures contribute mostly to the measured correlations, while those from the random fine-scale turbulence are not measurable (which may be simply due to a much larger population); 2) a strong low-frequency source is located on the jet axis downstream of the end of the potential core and extends several diameters beyond; and 3) the source on the jet axis has more radiative components than the one on the shear layer, even for supersonic jets.

Bogey and Bailly [36,37] investigated the characteristics of the noise sources in two unheated $M = 0.6$ and $M = 0.9$ jets using LES data. Correlations of the fluctuations from different locations of the jet with the pressures computed at two far-field microphone angles of approximately 90 and 153 deg captured the trends seen in the measurements of [34,35]. Specifically, the high correlations between the far-field pressure at the aft angle and a velocity component at points on the jet centerline downstream of the potential core were reproduced by LES. The simulations also supported the concept of two independent noise sources/mechanisms.

The results presented here cover a wide range of jet velocities. For the higher velocity jets, the convective Mach number is supersonic and there should be strong radiation from the large-scale structures. This component of noise may indeed be identified easily as the intense directional Mach wave emission seen in the pressure–time derivative plots for the high velocity jets in Figs. 6d and 21. As already noted, these figures (and the movies for these cases) indicate clearly that the acoustic waves originate from the shear layer, starting close to the nozzle exit. The second noise source is located on the centerline at $\sim 14D$ for $M = 1.9$ and $\sim 7.5D$ for the $M = 1.0$ heated jet. Thus, the current simulations pinpoint the presence of the two strong sources seen in the correlation measurements of [34,35] and the mirror measurements of [27].

The situation is different for low velocity jets. The shear layer source due to Mach wave radiation is absent, but there is a strong source on the centerline at $\sim 7.5D$. The location of this source is also in accord with the correlation and mirror measurements. A close examination of the snapshot of $(\partial p/\partial t)$ and the movie shows a directional radiation to the aft angles in addition to the circular waves. However, unlike for the high velocity jets, the wave fronts are almost normal to the jet axis and are confined to a very narrow angular range, close to the jet axis. In the annotated snapshot of $(\partial p/\partial t)$ in Fig. 15, the direction of these waves is indicated by the thick arrow from the observed source location. The two aft angles of 155 and 160 deg, with respect to the nozzle exit plane, are denoted by the crosses. It is clear that this directional component is confined to polar angles $\geq \sim 150$ deg. This is also the region where the spectral shapes are different and correspond to the LSS shape. It was hypothesized in [18] that the rapid nonlinear collapse of the instability waves

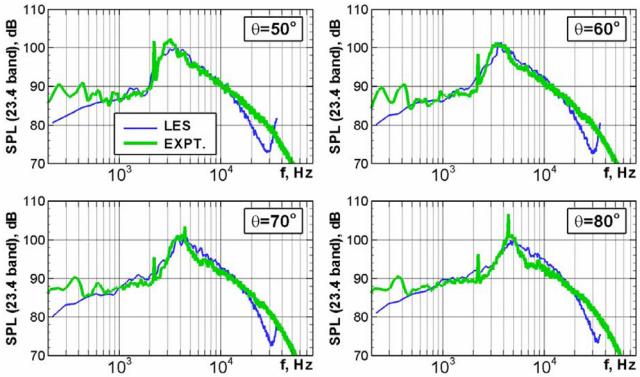

Fig. 26 Comparison of spectra with significant broadband shock-associated noise. $M = 1.56$, $T_t/T_a = 3.2$. Blue (thin lines): predictions; green (thick lines): data.

downstream of the potential core could be the physical mechanism responsible for the observed spectral shape at large aft angles. The LES data seem to support this point of view. Further analysis is necessary.

Figure 15 and the movie also indicate a source close to the nozzle exit. This could be a high-frequency source. One can also see this source and circular wave fronts, with propagation to the lower angles for the $M = 1.0$, $T_t/T_a = 3.2$ jet in the movie and in Fig. 6d, as well as for the $M = 1.9$ jets. However, due to the stronger Mach wave radiation for the $M = 1.9$ jets, the waves from this source are somewhat masked. Experiments to date have failed to measure the source component that radiates to the lower polar angles; however, the classical theories as well as the theory of Tam and Auriault [38] predict the noise generated by the fine-scale turbulence at the lower angles.

Currently there is no analytical method capable of predicting the entire spectra at aft angles. As discussed in Sec. II, theories based on variants of the acoustic analogy and simplistic synthetic turbulence do not predict the experimentally observed trends. The predictions from LES capture the physics, as attested to by the good spectral agreement with data at various jet velocities at all the angles. Clearly, new thinking on the sources of jet noise is needed; LES could perhaps provide guidance on developing a suitable theory.

C. Shock-Associated Noise

Finally, we show an example (underexpanded heated $M = 1.56$ jet) with significant broadband shock-associated noise. It is well known that the interaction of the large-scale turbulence with the shock cell system leads to an additional noise component. Comparisons with narrowband data from the convergent round nozzle are shown in Fig. 26. The predicted shock peak frequencies as well as the levels are very good at all the lower polar angles where shock-associated noise is dominant. The blips in the data at the lower frequencies, in the range of 200 to ~400 Hz are facility related and are not part of the jet noise spectra. However, these tones have not been removed and the as-measured spectra are shown (see [18,19] for more details). There is very good agreement up to a frequency of ~20 kHz ($St = 1.57$), which is the upper limit for the grids used. Absolute predictions of the shock-noise peak locations and levels, without any empirical adjustments, attest to the validity of the approach and indicate that the right physics is captured in the simulations.

V. Summary

The flow and the noise characteristics of round nozzles have been investigated, with the goal of gaining insights into the flow features that are responsible for noise generation and which can be altered for the purpose of noise reduction. The importance of rendering the nozzle internal flow, especially for complex geometries of interest and aircraft applications, has been emphasized. Large-eddy simulation of the entire internal and external flow is not practical in the foreseeable future; therefore, a two-step approach in which the LES is provided information from a RANS simulation has been developed and applied to a variety of nozzle geometries [15]. The combined RANS/LES method involves a RANS solution of the entire flowfield as a precursor, with the LES of only the external plume performed for noise prediction in the second step. The RANS computations provide the inflow conditions, the crucial inputs for any simulation, with realistic resolution of the boundary layers, Reynolds averaged of course, inside the nozzle. This step replaces the manual specification of the inflow conditions, which is not sufficiently accurate for realistic geometries.

An incisive analysis of jet noise data was first presented. The Doppler factor $[1 - M_c \cos(\xi)]$ figures prominently in the classical theories of jet noise (which are based on the idea of moving sources), both for scaling frequency and for calculating the spectral shapes at aft angles, with a presumed known shape at 90 deg. The role of this term in both these respects has been critically reviewed here and in [20]. Excellent spectral collapse at various aft angles was demonstrated *without* the Doppler factor, using the scaling laws developed by Viswanathan [19]. It was shown unambiguously that once the importance of the jet temperature ratio is explicitly accounted for, perfect collapse over the entire frequency range is possible at all angles using plain Strouhal scaling. Further, the jet temperature ratio, rather than the convective Mach number (M_c), controls the spectral shape at aft angles. As seen in Fig. 3, heated jets with a lower M_c have a sharper peak than an unheated jet at a higher M_c (see also [20]). Therefore, the concept of convective amplification and flow/acoustic interaction appears insufficient to explain, let alone predict quantitatively, the change in spectral shape observed with increasing radiation angle seen in Fig. 1. These experimental results point to the role of the large-scale highly anisotropic turbulence structures in the flow for the observed variations in spectral shape, which of course supports the rationale for LES.

Large-eddy simulations have been carried out to understand the dynamics of the large- and medium-scale turbulence structures in noise generation. First of all, it is highlighted that good spectral agreement with measured data has been achieved for a wide range of jet velocities from 440 ft/s (134 m/s) to 2770 ft/s (845 m/s), obtained from unheated $M = 0.4$ and 0.9 jets, highly heated $M = 0.6$ and 1.0 jets, and unheated and heated $M = 1.9$ jets. Absolute predictions, without any empiricism, yield noise levels in most cases within approximately 2–3 dB of data over this velocity range. These good spectral predictions signify that the correct physics is captured and give confidence that the interpretations of the flow/noise solutions are meaningful. The higher velocity $M = 1.0$ and 1.9 jets are convectively supersonic ($M_c > 1.0$). Snapshots and movies of $(\partial p/\partial t)$ clearly indicate Mach wave radiation for these jets, and there is extensive experimental and analytical evidence for this noise component. This source of noise is generated at the jet shear layer, starting close to the nozzle exit. There is another noise source located on the jet centerline, at $\sim 7.5D$ and $\sim 14D$ for the $M = 1.0$ and 1.9 jets, respectively. The predicted source locations are in good agreement with elliptic mirror measurements.

The results for the lower Mach number jets are relevant to debates over different spectral shapes. The data indicate that the shapes at angles close to the jet axis have the LSS shape with a narrow peak, much like at higher Mach numbers (see Figs. 13 and 19). The distinct spectral shapes at aft angles, as well as the gradual change in shape with increasing angle (from 90 deg), are captured by LES for all jet velocities. There is no Mach wave radiation for these jets, M_c being far below 1. The instantaneous $(\partial p/\partial t)$ plot and movie for the $M = 0.4$ unheated jet show a strong source on the jet axis at $\sim 7.5D$. Whereas the source on the jet centerline has an elongated shape for the high velocity jets, it is more compact for this case. Almost omnidirectional circular wave fronts emanate from this source; in addition, there is beaming of directional radiation to aft angles. This directional radiation is confined to angles $\geq \sim 150$ deg (see bottom plot of Fig. 15). Spectral analysis indicates that the spectra within this sector have the LSS shape, with a low-frequency peak. Viswanathan [18] pointed out that the instability waves at low Strouhal numbers amplify more gradually than waves at high Strouhal numbers and attain their peak amplitudes close to the end of the potential core. In addition, waves in low velocity jets have higher growth rates than

those of high-speed jets. Just beyond the potential core, these waves have no mechanism to extract energy from the mean flow and lose their energy through nonlinear processes. This process would occur over a region that is a few diameters in extent, downstream of the end of the potential core. The modulation of the amplitude of the waves could trigger low wave number components with potentially supersonic phase speeds relative to the ambient speed of sound. This mechanism is needed to understand noise radiation at this low Mach number in terms similar to those which are well accepted at much higher convective Mach numbers. Given the low velocities, though, this radiation would be confined to angles close to the jet axis. Thus, the large-scale structures could be a source of noise for low velocity jets as well. The physical process outlined here could also explain the puzzling observation of why the LSS shape, extracted from jets with velocities of 3450 ft/s (1050 m/s), is seen for such a low velocity jet (in which the prima facie convective Mach number is completely unable to predict any significant changes). As noted above, the LES results pinpoint a strong source at $\sim 7.5D$, which is $\sim 3D$ downstream of the end of the potential core, with directional radiation confined to angles close to the jet axis. Therefore, LES provides corroborating evidence for the hypothesis proposed by Viswanathan [18]. A more detailed investigation is underway. This is precisely the kind of information and insights that LES can provide, which is hard to obtain in experiments.

The results presented here are part of an ongoing effort to gain a better understanding of the flow physics; several simulations are underway for both round and beveled nozzles. Results from these studies will be reported in the future. The ability to relate subtle changes in the flow to noise remains a never-ending quest and a fruitful area for research.

Acknowledgment

The authors from New Technologies and Services (NTS) were partially supported by the Russian Basic Research Foundation, under Grant No. 06-08 00358.

References

[1] Lighthill, M. J., "On Sound Generated Aerodynamically: I. General Theory," *Proceedings of the Royal Society of London, Series A: Mathematical and Physical Sciences*, Vol. 211, 1952, pp. 564–581.

[2] Bogey, C., and Bailly, C., "Investigation of Subsonic Jet Noise Using LES: Mach and Reynolds Number Effects," AIAA Paper 2004-3023, May 2004.

[3] Bogey, C., Bailly, C., and Juve, D., "Noise Investigation of a High Subsonic, Moderate Reynolds Number Jet Using a Compressible LES," *Theoretical and Computational Fluid Dynamics*, Vol. 16, No. 4, 2003, pp. 273–297.

[4] Andersson, N., Eriksson, L. E., and Davidson, L., "Large Eddy Simulation of Subsonic Turbulent Jets and Their Radiated Sound," *AIAA Journal*, Vol. 43, No. 9, 2005, pp. 1899–1912.

[5] Bodony, D. J., and Lele, S. K., "Review of the Current Status of Jet Noise Predictions Using Large-Eddy Simulation," AIAA Paper 2006-486, Jan. 2006.

[6] Uzun, A., Lyrintzis, A. S., and Blaisdell, G. A., "Coupling of Integral Acoustics Methods with LES for Jet Noise Prediction," *International Journal of Aeroacoustics*, Vol. 3, No. 4, 2005, pp. 297–346.

[7] Lew, P., Blaisdell, G. A., and Lyrintzis, A. S., "Recent Progress of Hot Jet Aeroacoustics Using 3-D Large Eddy Simulations," AIAA Paper 2005-3084, May 2005.

[8] Paliath, U., and Morris, P. J., "Prediction of Noise Form Jets with Different Nozzle Geometries," AIAA Paper 2004-3026, May 2004.

[9] Paliath, U., and Morris, P. J., "Prediction of Jet Noise from Circular Beveled Nozzles," AIAA Paper 2005-3096, May 2005.

[10] Rahier, G., Prieur, J., Vuillot, F., Lupoglazoff, N., and Biancheirn, A., "Investigation of Integral Surface Formulations for Acoustic Post-Processing of Unsteady Aerodynamic Jet Simulations," *Aerospace Science and Technology*, Vol. 8, No. 6, Sept. 2004, pp. 453–467.

[11] Vuillemin, A., Loheac, P., Rahier, G., Vuillot, F., and Lupoglazoff, N., "Aeroacoustic Numerical Method Assessment for a Double Stream Nozzle," AIAA Paper 2005-3043, May 2005.

[12] Ffowcs-Williams, J. E., and Hawkings, D. L., "Sound Generated by Turbulence and Surfaces in Unsteady Motion," *Philosophical Transactions of the Royal Society of London, Series A: Mathematical and Physical Sciences*, Vol. 264, No. 1151, 1969, pp. 321–342.

[13] Shur, M. L., Spalart, P. S., and Strelets, M., "Noise Prediction for Increasingly Complex Jets. Part 1: Methods and Tests," *International Journal of Aeroacoustics*, Vol. 4, Nos. 3, 4, 2005, pp. 213–246.

[14] Shur, M. L., Spalart, P. S., and Strelets, M., "Noise Prediction for Increasingly Complex Jets. Part 2: Applications," *International Journal of Aeroacoustics*, Vol. 4, Nos. 3, 4, 2005, pp. 247–266.

[15] Shur, M. L., Spalart, P. S., Strelets, M., and Garbaruk, A. V., "Further Steps in LES-Based Noise Prediction for Complex Jets," AIAA Paper 2006-485, Jan. 2006.

[16] Viswanathan, K., "Nozzle Shaping for Reduction of Jet Noise from Single Jets," *AIAA Journal*, Vol. 43, No. 5, 2005, pp. 1008–1022.

[17] Viswanathan, K., "An Elegant Concept for Reduction of Jet Noise from Turbofan Engines," *Journal of Aircraft*, Vol. 43, No. 3, May–June 2006, pp. 616–626.

[18] Viswanathan, K., "Aeroacoustics of Hot Jets," *Journal of Fluid Mechanics*, Vol. 516, Oct. 2004, pp. 39–82.

[19] Viswanathan, K., "Scaling Laws and a Method for Identifying Components of Jet Noise," *AIAA Journal*, Vol. 44, No. 10, Oct. 2006, pp. 2274–2285.

[20] Viswanathan, K., "Does a Model Scale Nozzle Emit the Same Jet Noise as a Jet Engine?," *AIAA Journal* (to be published).

[21] Tam, C. K. W., Golebiowski, M., and Seiner, J. M., "On the Two Components of Turbulent Mixing Noise from Supersonic Jets," AIAA Paper 96-1716, 1996.

[22] Tam, C. K. W., "Jet Noise Generated by Large-Scale Coherent Motion," *Aeroacoustics of Flight Vehicles: Theory and Practice, Volume 1: Noise Sources*, edited by H. H. Hubbard, NASA RP-1258, 1991, pp. 311–390.

[23] Ffowcs-Williams, "The noise from turbulence convected at high speed," *Philosophical Transactions of the Royal Society of London, Series A: Mathematical and Physical Sciences*, Vol. 255, 1963, pp. 469–503.

[24] Lilley, G. M., "Aerodynamic Noise," *Noise Mechanisms*, AGARD CP-131, 1974, pp. 13.1–13.12.

[25] Strelets, M. K., "Detached Eddy Simulation of Massively Separated Flows," AIAA Paper 2001-0879, Jan. 2001.

[26] Viswanathan, K., and Clark, L. T., "Effect of Nozzle Internal Contour on Jet Aeroacoustics," *International Journal of Aeroacoustics*, Vol. 3, No. 2, 2004, pp. 103–135.

[27] Viswanathan, K., "Investigation of the Sources of Jet Noise," AIAA Paper 2007-3601, May 2007.

[28] Lau, J. C., Morris, P. J., and Fisher, M. J., "Measurements in Subsonic and Supersonic Free Jets Using a Laser Velocimeter," *Journal of Fluid Mechanics*, Vol. 93, No. 1, 1979, pp. 1–27.

[29] Lau, J. C., "Effects of Exit Mach Number and Temperature on Mean-Flow and Turbulence Characteristics in Round Jets," *Journal of Fluid Mechanics*, Vol. 105, 1981, pp. 193–218.

[30] Arakeri, V. H., Krothapalli, A., Siddavaram, V., Alkislar, M. B., and Lourenco, L. M., "On the Use of Microjets to Suppress Turbulence in a Mach 0.9 Axisymmetric Jet," *Journal of Fluid Mechanics*, Vol. 490, 2003, pp. 75–98.

[31] Lilley, G. M., "Jet Noise Classical Theory and Experiments," *Aeroacoustics of Flight Vehicles: Theory and Practice, Volume 1: Noise Sources*, edited by H. H. Hubbard, NASA RP-1258, 1991, pp. 211–289.

[32] McLaughlin, D. K., Morrison, G. L., and Troutt, T. R., "Experiments on the Instability Waves in a Supersonic Jet and Their Acoustic Radiation," *Journal of Fluid Mechanics*, Vol. 69, No. 1, May 1975, pp. 73–95.

[33] McLaughlin, D. K., Morrison, G. L., and Troutt, T. R., "Reynolds Number Dependence in Supersonic Jet Noise," *AIAA Journal*, Vol. 15, No. 4, 1977, pp. 526–532.

[34] Panda, J., and Seasholtz, R. G., "Experimental Investigation of Density Fluctuations in High-Speed Jets and Correlations with Generated Noise," *Journal of Fluid Mechanics*, Vol. 450, 2002, pp. 97–130.

[35] Panda, J., Seasholtz, R. G., and Elam, K. A., "Investigation of Noise Sources in High-Speed Jets via Correlation Measurements," *Journal of Fluid Mechanics*, Vol. 537, 2005, pp. 349–385.

[36] Bogey, C., and Bailly, C., "Investigation of Sound Sources in Subsonic Jets Using Causality Methods on LES Data," AIAA Paper 2005-2885, May 2005.

[37] Bogey, C., and Bailly, C., "Investigation of Downstream and Sideline Subsonic Noise Using Large Eddy Simulation," *Theoretical and Computational Fluid Dynamics*, Vol. 20, No. 1, 2006, pp. 23–40.

[38] Tam, C. K. W., and Auriault, L., "Jet Mixing Noise from Fine-Scale Turbulence," *AIAA Journal*, Vol. 37, No. 2, 1999, pp. 145–153.

C. Bailly
Associate Editor